Alexander Eibel, BSc

Poly(2-oxazoline)-based Nanocomposites for High-Voltage Applications

MASTERARBEIT

zur Erlangung des akademischen Grades

Diplom-Ingenieur

Masterstudium Technische Chemie

eingereicht an der

Technischen Universität Graz

Betreuer

Priv.-Doz. Dipl.-Chem.Univ. Dr.rer.nat. Frank Wiesbrock

Institut für Chemische Technologie von Materialien

Graz, Februar 2017

EIDESSTATTLICHE ERKLÄRUNG

Ich erkläre an Eides statt, dass ich die vorliegende Arbeit selbstständig verfasst, andere als die angegebenen Quellen/Hilfsmittel nicht benutzt, und die den benutzten Quellen wörtlich und inhaltlich entnommenen Stellen als solche kenntlich gemacht habe. Das in TUGRAZonline hochgeladene Textdokument ist mit der vorliegenden Masterarbeit identisch.

Datum 08.06.2017 Unterschrift 

STATUTORY DECLARATION

I declare that I have authored this thesis independently, that I have not used other than the declared sources / resources, and that I have explicitly marked all material which has been quoted either literally or by content from the used sources.

Date 01.06.2017 Signature 

Danksagung

Die vorliegende Forschungsarbeit wurde in den K-Projekten ‚PolyComp' und ‚PolyTherm' an der Polymer Competence Center Leoben GmbH im Rahmen des COMET-Programms des Bundesministeriums für Verkehr, Innovation und Technologie und Bundesministeriums für Wissenschaft, Forschung und Wirtschaft unter Beteiligung des Instituts für Chemische Technologie von Materialien der TU Graz und des Department Electrical Sustainable Energy der Delft University of Technology erstellt und mit Mitteln des Bundes und des Landes Steiermark gefördert.

Ich möchte mich an erster Stelle bedanken bei Herrn Priv.-Doz. Dipl.-Chem.Univ. Dr.rer.nat. Frank Wiesbrock und Herrn Em.Univ.-Professor Dipl.-Ing. Dr.tech. Franz Stelzer für ihre wohlwollende Unterstützung, fachliche Hilfestellung und lehrreiche Zeit bei der Durchführung dieser Arbeit. Ein herzlicher Dank gilt Huifei Jin für die Messungen der elektrischen Eigenschaften der Proben. Ebenso danke ich Josefine Hobisch für die GPC-Messungen und Petra Kaschnitz für Ihre Unterstützung bei den NMR-Anaylsen.

Meinen herzlichen Dank möchte ich auch an meine Kollegen und Kolleginnen der Arbeitsgruppe aussprechen, allen voran Klaus Luef, Robin Hoffmann, Martin Rausch, Zucong Zhang, Florian Mostegel und Elisabeth Rossegger für ihren Rat und Unterstützung. Des Weiteren möchte ich den Kollegen und Kolleginnen des ICTM danken, welche mich teilweise vom Studienanfang an begleitet haben und die ich an dieser Stelle namentlich erwähnt haben möchte: Birgit Ehmann, Lukas und Bettina Schafzahl, Katrin Niegelhell, Nicole Steinmann und Patrick Posch.

Einen besonderen Dank möchte ich an meine Familie richten, die mir zu jeder Zeit einen starken Rückhalt geboten hat und die mir alle Energie zukommen hat lassen. Danke an meine Eltern Josefa und Siegfried, sowie meiner Schwester Claudia!

Danke auch an Christina, für Deine tolle Unterstützung, Deinen Rückhalt und die wunderbare Zeit die wir miteinander haben!

Table of content

1. Introduction

The currently used power-supply systems will face increasing challenges in the upcoming years, as industry increases their energy demand, which is mostly to be provided by electricity. Austria is one of the internationally leading countries in producing energy from renewable resources. However, due to the inconsistent nature of energy generation from renewable resources such as wind power, hydroelectric power and solar power, sometimes surplus electricity is generated as well as, on the other hand, too low amounts of electricity may be produced. Austria uses surplus electricity, e.g., to store water in heightened positions with pumped storage plans. This water can be used to generate electricity with generator-turbines.[1] The recent generation of generators is manufactured from high-end materials such as epoxy-based resins, which are used as insulation materials. Polymers and polymer-based composites are commonly used as electrical insulators.[2] There are some dielectric requirements which every insulator must fulfil, such as a high dielectric strength, low dielectric losses and a good tracking resistance. Also, mechanical properties like the elastic module, tensile strength and toughness are targeted. For outdoor applications, low moisture adsorption, low or non-swelling in water and a good weather resistance are required.[3] Epoxy-based resins are easy to handle, have a low density, high dielectric strength, and their blending with additives is easy.[4]

In order to further improve the properties of polymers for high-voltage applications, first micro-particles and, in recent years, nanoparticles were added to the polymer matrices. Recently, more and more researchers have drawn attention to nanocomposites. A general definition of a composite is the combination of two or more materials with the objective to get a more favorable combination of properties. In the case nanocomposites, one or more phases with nanoscaled dimensions are embedded in a polymer matrix.[5] In most recent literature, nanoparticles are defined to bear particle sizes between 10 and 100 nm (smaller than 500nm). Under these conditions, a large interface between the matrix (e.g., a polymer) and the nanoparticles is formed. This huge interface

brings some advantages which cannot be realized with traditional additives, for example to increase the toughness, module and strength.[6] Additional properties that potentially can be influenced by nanoparticles are the dielectric strength, tracking and erosion resistance, the dielectric loss and the hydrophobicity of the surface.[7] Another major point of interest is to enhance the thermal conductivity, for which highly conducting particles are to be used as thermal interface.[8] Evans and colleagues found some key factors, which are effecting the thermal conductivity, like the filler shape and the dispersion/aggregation state of the nanofluids and solid composites.[8]

A serious health concern of epoxy-based resins is the effect of non-polymerized monomer bisphenol A on the human hormonal system, as there are structural resemblances between bisphenol A and the hormone oestrogen.[9,10] The European Commission has adopted a regulation for specific applications of epoxy-based resins starting in the year 2020. Within this framework, alternative polymers for the replacement of these components have to be found.[11]

In recent years, the polymer class of poly(2-oxazoline)s drew the interest of research groups working on this particular topic due to the benefits of this polymer class, like the large spectrum of different monomers to choose from for the synthesis of the corresponding copoly(2-oxazoline)s. With these large variety of monomers, copolymers with tailor-made properties such as the polarity of the polymer, its hydrophobic or hydrophilic behaviour, surface roughness, or functional groups occurring at the side-chains for further polymeranalogous modifications can be obtained.[12] Another advantage of the poly(2-oxazoline)s is that several congeners can be synthesized from renewable resources.[13] Due to various functional groups of the side-chains from the poly(2-oxazoline)s, it is possible to generate 3D networks.[14] The 3D networks can be created via different click-chemistry reactions[15], of which one of the better known and highly efficient examples is the UV-induced thiol-ene click reaction.[16]

2. Scope and Motivation

The motivation of this current work was to investigate poly(2-oxazoline)-based nanocomposites as possible replacement for epoxy-based resins in the field of high-voltage insulation media. For the synthesis of the 2-oxazoline monomers, the reactants should be chosen from renewable resources and provide the functional groups for a click chemistry approach such as the UV-mediated thiol-ene click reaction for polymeranalogous crosslinking. The monomers and the copoly(2-oxazoline)s should be synthesized according to well established and already published protocols. After manufacturing copoly(2-oxazoline)-based networks, the next cornerstone was the production of nanocomposites based on these copoly(2-oxazoline)s with a well-defined shape and thickness.

For future application as insulation materials, different properties had to be investigated: The dielectric breakdown strength indicates the maximum voltage that can be applied to the insulator. The relative permittivity quantifies the capacity of the material to store energy. This parameter should be approximately zero, since an insulator does not store energy. The thermal conductivity is an important criterion for transformers considering approaches for a more compact design of such machinery, while heat is generated during operation. Differential scanning calorimetry enables for a better understanding of the morphology in the nanocomposites. Moisture adsorption was quantified as high water uptake can generate short-circuits and accelerate degradation.

The nanoparticles used in this thesis needed to fulfil certain requirements such as electric insulation, high thermal conductivity and commercial availability. Nanoparticles that meet these requirements are (native) silica,[17] (native) alumina,[18] (native and modified) boron nitride,[19] and (modified) nanodiamonds – all these types of nanoparticles were used in this study aiming to improve the properties of the corresponding composites.

3. State-of-the-Art

3.1 High-Voltage Technology

In the 19th century, Ernest Werner Siemens, who is known as the founder of modern electrical engineering, invented the first generator.[20] A couple of years later, a patent for an alternating current generator was applied for by Nikola Tesla.[21] These were two of the most important inventions for modern society, as they constitute the fundamental base of our power supply system. Transformers enable the transfer of electricity over long distances without big losses. These technologies allowed the construction of power supplies outside of cities as well as the transfer of electrical power over long distances. The high voltage in the overhead lines and the transformers needs to be insulated. To avoid blackouts (caused additionally by, e.g., lightning strokes on the overhead lines) the research field of high-voltage engineering was born. Typical applications of high-voltage technology comprise wind power, high-voltage cables, photovoltaic systems, arc melting furnaces, power converters for electric drives, transformers, generators, converters, power supplies for industry, or single-phase parallel couplings for the public mains supply.[22]

One of the most significant goals of the high-voltage technology is to control the high electric field strength over long distances. High electric field strength applies not only at high-current devices, but also at low current devices with reduced insulation. In recent years, high-voltage direct current HVDC technology has been often used for intercontinental power transmission. High-voltage overhead lines are only possible due to the insulating properties of gases such as sulphur hexafluoride, SF_6 or air. Due to costs and the relative permittivity of 1,[23] specific air is the commonly used insulation material. However, above 30 $kV \cdot cm^{-1}$ air gets ionized and leads to a high short-circuit current. Hence, in transformers, solid insulation materials such as glass, porcelain and polymers are used as well in combination with liquid insulators such as mineral oil.[23] The

electrical stress of the electric field *E* must be significantly below the dielectric strength E_d (Formula 1).[22]

$$E \ll E_d \quad (1)$$

In recent years, the so-called 'high voltage-directed-transmission' has received attention. This technique requires a point-to-point transmission where the voltage is limited by 1 million volts. The power loss is lower than 3% over a distance of 1000 km, compared to the power loss of other techniques of ~10% over the same distance.[24]

3.2 Transformers and Generators

3.2.1 Transformers

An electrical power transformer is a key component for any electrical service network, because power transformers change the voltage stepwise to higher or lower voltage.[25] The general aim of power transformers is to switch the voltage level from one to another. The copper windings have to be capable of handling the full load of current, overcurrent and magnetic current, so does the insulation.

Transformers are built of linked coils, in which conducting wires are wrapped around a ferromagnetic core and protected with paper-based insulators. The production of transformers in an oil bath started in the year 1912; the oil bath serves simultaneously as insulating and cooling agent. A major challenge concerning the oil bath is the flammability of the media, which was compensated for in first approaches by the addition of polychlorinated biphenylene PCB. In the 1980´s, the production of PCB was discontinued due to health risks of this compound (such as pathological changes in the immune response, birth defects, or cancer). Starting in the 1960´s, cast-resin transformers were produced. In these

machines, the wire is wrapped around the reel and into the cast-resin under vacuum. The different models of transformers may be distinguished into one-phase, three-phase and rotating-transformers. One-phase transformers are special transformers for the industry and railway power supply. Three-phase transformers can have a special constructed core or are a combination of three one-phase transformers.[26]

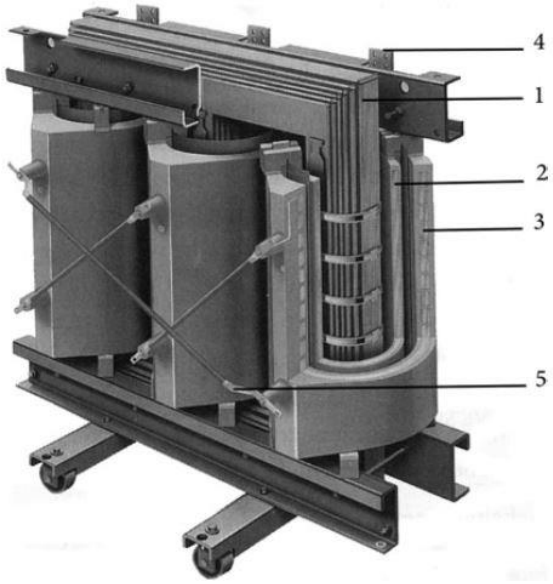

Figure 1: Scheme of a case resin transformer.[26] 1: Iron core; 2: low voltage winding; 3: high voltage winding; 4: low voltage connection; 5: high voltage connections

3.2.2 Generators

The physical concept of a generator is to transfer mechanical work to electrical energy. For the working principle of a generator, only a magnetic field or electromagnets placed around a rotating coil are needed (Figure 2), such that electric current is induced.[27] It is possible to generate AC or DC power. Generators are most likely powered by a fuel engine in their application as emergency power.

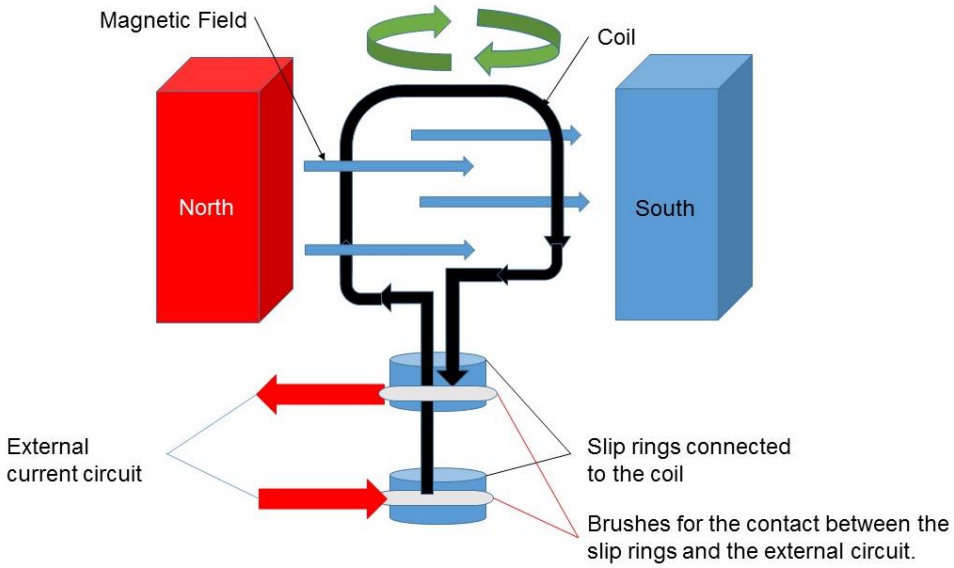

Figure 2: Electrical power generator.

A typical generator has a voltage of 24 kV, and large generators typically operate in the range between 500 and 900 MVA. The full lead current of such generators is in the order of 10 to 20 kV, which makes cooling of the system necessary (Figure 3) due to the high currents. Due to the limited space between each stator wing, the insulation material has to fulfil high demands (Figure 4).[23]

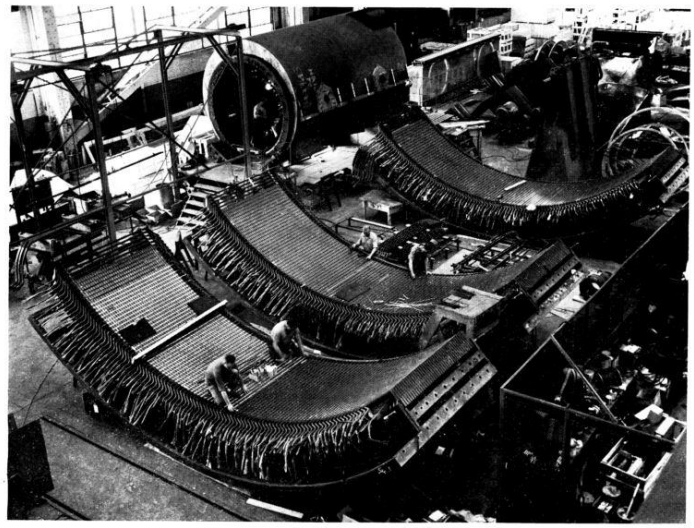

Figure 3: High voltage generator.[28]

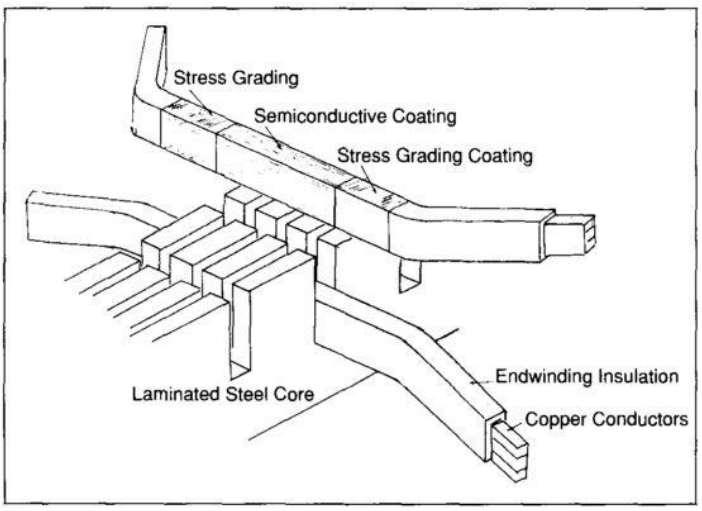

Figure 4: Cross-section of a stator wing.[29]

3.3 Epoxy-based Resins

Cyclic ethers with a three-atom ring containing one oxygen heteroatom are called epoxides (Figure 5). Due to its equilateral triangular shape, the ring is under high strain and, correspondingly, epoxides are highly reactive and easily undergo ring-opening reactions upon nucleophilic attack. The ring-opening reactions may be acid- or base-catalysed and can occur according to S_N2 or S_N1 reaction mechanisms.[30]

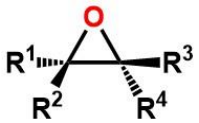

Figure 5: Chemical structure of epoxides.

Epoxy-based resins are widely used in different ways such as outdoor, indoor and enclosed applications.[7] According to Chonkaew et al., the favourable characteristics of epoxy-based resins comprise high chemical and corrosion resistance, good mechanical and thermal properties, low shrinkage upon cure, good electrical properties, flexibility, good adhesion

to various substrates, and easy processability.[31] However, there are some disadvantages such as moisture adsorption, brittle nature of the crosslinked congeners, high-water uptake, high friction coefficient, and low wear resistance.[31]

There are two routes for the synthesis of epoxy-based resins. The direct synthesis starts from an olefin that is oxidized to an epoxide by peroxides, while the indirect method starts from an epoxide with functionalized groups.[32]

If no hardeners such as anhydrides or amines are added, the polymerization of epoxides may start from the ring-opening reaction of the epoxide epichlorohydrine with Bisphenol A (Figure 6). In alkaline solution, oxygen anions are formed by the abstraction of hydrogen atoms from the phenolic OH groups, which attack the epichlorohydrines. After the polyaddition (Figure 6), a duroplast is formed.[37,4] Upon the condensation of water and sodium chloride, novel epoxide moieties are formed for subsequent chain-growth reactions.

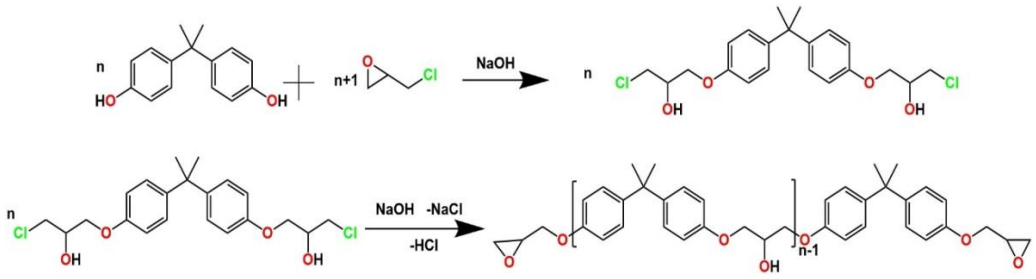

Figure 6: Schematic representation of the chain-growth of epoxy resins.

Depending on the amount of epichlorohydrine, the viscosity and chain length of the epoxy resin can be adjusted. If epichlorohydrine is used in high excess, a low-molecular weight low-viscous epoxy-based resin is formed. If epichlorohydrine is used in small excess, a high-molecular weight high-viscous epoxy-based resin is formed due to multiple reactions with Bisphenol A.

Without a hardener, this condensation reaction only yields to pre-products for industrial applications. Hardeners such as anhydrides or amines react with the epoxy groups and build bridges between the resins; they act, however, neither as initiator nor as catalyst. Amines are used for cold hardening (not necessarily requiring initiators nor catalysts), and anhydrides are used for warm hardening (requiring 'activators'). Commonly, for industrial applications, epoxy resins systems are supplied with additional hardeners either as one- or two- component systems. Amine-hardened epoxy resins, e.g., are (at least) two-component systems comprised of the epoxy component such as, e.g., Bisphenol A/F diglycidylether and a hardener component composed of amines and/or polyamines. Eventually, a third component composed of a reactive diluent (e.g. glycidic ethers) is added.

For their application as insulation materials, epoxy resins must fulfil a variety of properties as not only electrical stress but also mechanical and thermal stress are applied. The mechanical stress is due to the force exerted by the flow of high current or the vibration stress which leads back to mechanical motion.[33] Hence, in order to further improve the insulation properties of epoxy resins, fillers are added, which have a positive influence on the composite properties due to their thermal, mechanical and chemical properties.[34] Wetzel and co-workers presented the enhancement of the mechanical properties of epoxy resins by increasing the crosslinking density, which leads to a higher stiffness and strength. The disadvantage of this approach is higher brittleness due to plastic deformation. Another side-effect of the local stress is the formation cracks, in which spontaneous insulation failure can occur. The aim to develop epoxy resins with higher toughness without narrowing other important characteristics such as elastic modulus, and thermo-mechanical properties has been tried with a variety of toughening agents such as spherical rubber particles, liquid rubbers, glass beads, micro-voids, hyperbranched polymers, core shell particles or combinations of these.[35] In recent time, different studies have shown that the usage of nanoparticles as filler materials has an advantage over particles of the micrometre scale;

compared to micro-filled materials the use of nano-filled materials may provide superior performance.[7]

3.3.1 Bisphenol A (BPA)

Bisphenol A BPA is one of the chemical compounds with the highest production volume in the world. The applications of BPA are numerous and range from building blocks in epoxy resins, food packaging, coatings of DVDs to its employment in the automobile industry or sports safety equipment. In the early 1930´s, BPA was also used as a synthetic oestrogen. Recent studies showed that a detectable amount of BPA was found in 92.6% of trail participants.[9] BPA was also found in the human blood stream, serum, and placental tissue. Although BPA has a 10.000 to 100.000 weaker affinity to oestrogen receptors than oestrogen itself, studies have shown that BPA can stimulate cellular response at low concentrations through a variety of pathways. There are some conditions in women related to the BPA level such as endometrial hyperplasia, abnormal karyotypes recurrent miscarriages, polycystic ovarian syndrome, and obesity. Another study found a link between BPA and chromosomal abnormalities.[10] For all these side-effects, the European Commission will ban BPA from food industry starting in the year 2020.[11]

3.3.2 Nanocomposites

In one common definition of nanomaterials, they are defined as a combination of two or more separate components, combining the best properties of each component. A nanocomposite, hence, consists of a matrix, usually a polymer, to which nanoparticles are added as fillers.[36] According to Hanemann and colleagues, material and structures with a size under 100 nm will gain ongoing attention within the scientific world. Nanoparticles are particles with a diameter below 100 nm, however, ideal nanoparticles have diameters in the range of 10 to 20 nm. An expanded definition of nanoparticles focuses on the properties of the particle, which

have a direct dependency on the size of the particle. The surface of the particles is a very important parameter, as the surface:volume ratio increases tremendously with decreasing particle size. A particle with, e.g., 5 nm has roughly 1000 atoms, so there are almost 40% of the atoms located at the surface of the particles.[37]

Correspondingly, the surface properties, physical properties, agglomeration behaviour and interfacial properties become more important with decreasing size of particles. 50 kg of a single crystal cube of SiO_2 have an edge length of 27 cm and a surface area of 0.44 m² (Figure 7). By comparison, the reduction to an edge length of 5 nm of the single crystal yields a surface area of 2 km² of the 50 kg charge. The physical property of polymer composites can be tailored by the addition of different types of fillers.

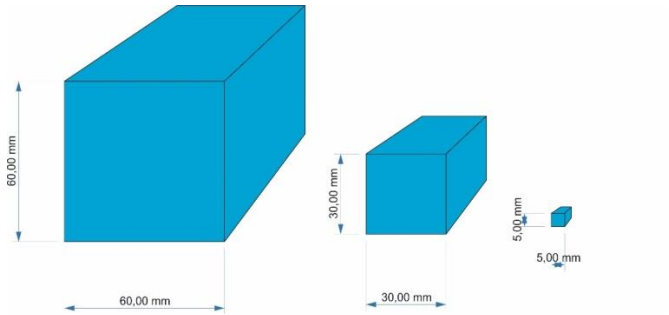

Figure 7: Correlation of particle sizes and surface areas: $60^2 \cdot 6 = 21.6$ cm^2; $30^2 \cdot 6 \cdot 2^3 = 43.2$ cm^2; $5^2 \cdot 6 \cdot 12^3 = 259.2$ cm^2.

With the addition of nanofillers, new applications can be realized. However, nanoparticles have a tendency to form agglomerates and this tendency depends strongly on surface chemistry and synthesis conditions.[37] Therefore, the challenge will be to realize a high filled and homogeneous composite. To increase the ductility, for example, epoxy resins are filled with thermoplastic particles, which tend to promote micro-cracking as well as crack bridging effects. The toughening mechanisms for filled epoxy resins include void formation around the particles and particles-matrix debonding, followed by the formation of ligaments. In recent time, research on low and high ratios of nanoparticles has already

shown their capability to improve properties such as electrical resistivity, wear resistance and the toughness of polymers.[35]

3.4 2-Oxazolines

In the past 15 years, concomitant with the introduction of microwave reactors for chemical syntheses, the interest in 2-oxazolines has (re-)grown constantly. This interest is based on the large variety of monomers of that polymer class. The general structure of 2-oxazolines is a heterocyclic five-membered ring with an oxygen and a nitrogen heteroatom at position 1 and 3, a double bond between a nitrogen and a carbon atom, and a substituent at the carbon atom at position 2 (Figure 8).

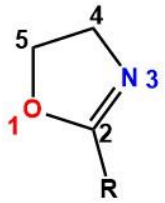

Figure 8: Chemical structure of 2-oxazolines.

3.5 Synthesis of 2-Oxazoline Monomers

In the year 1889, 2-oxazolines were successfully synthesized by Gabriel for the first time.[38] Nowadays, a couple of well-established synthesis strategies exist. The easiest and most common ways are so called ‘one-pot’ syntheses. According to the protocol described in the Henkel-patent[39] or by Witte and Seelinger[40], carboxylic acids or nitriles are converted to 2-oxazolines by the reaction with 2-aminoalcohols. This reaction is optimized for monomers with more than four carbon atoms in the side-chain. For the synthesis of monomers with a shorter side-chain, a multiple-step synthesis must be performed.[41]

3.5.1 Synthesis of 2-Oxazoline Monomers according to Witte and Seelinger

The synthesis according to Witte and Seelinger[40] is a one-step reaction of nitriles and 2-aminoethanol to 2-oxazolines. It is performed under nitrogen atmosphere with catalysts such as cadmium acetate dehydrate or zinc chloride at temperatures above 130 °C (

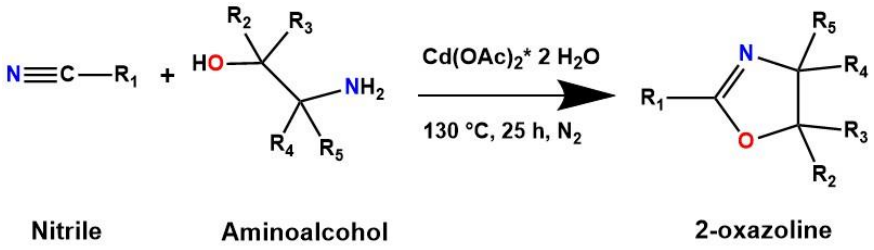

Figure 9). The reaction can be carried out without additional solvents. A complex apparatus for synthesis is necessary due to the formation of ammonia gas as side-product. The reaction must be stirred for 25 h at 130 °C. Afterwards, the product has to be distilled for purification.

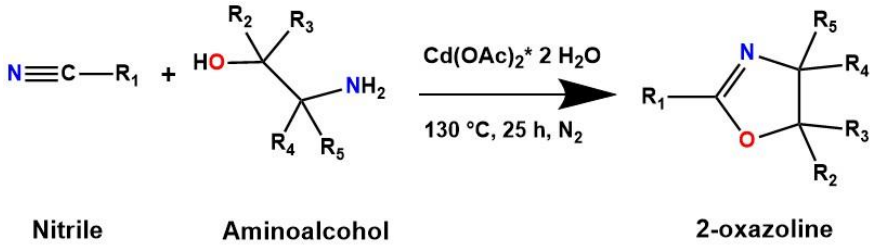

Figure 9: Schematic representation of the synthesis of 2-oxazolines according to Witte and Seelinger.

3.5.2 Synthesis of 2-Oxazline Monomers via the Henkel Patent

The Henkel patent[39] describes a synthesis, according to which fatty acids can be reacted with amino alcohols in the presence of a catalyst based on tetravalent titanium $Ti(OR)_4$ or zirconium $Zr(OR)_4$ compounds to yield 2-alkyl-2-oxazolines or 2-alkenyl-2-oxazolines (Figure 10). As by-product of the conversion of fatty acids and 2-aminoethanol, water is formed. Correspondingly, an inert gas atmosphere is not necessary. This

synthesis has the advantage that the catalyst titanium(IV)butoxide is more environmentally friendly than cadmium acetate from the synthesis of Witte and Seeliger. The product is separated and purified by vacuum distillation. The fatty acids for the Henkel synthesis can be obtained from renewable resources such undec-10-enoic acid from castor oil or decanoic acid from coconut oil; the base product for ethanolamine is the amino acid serine.[13]

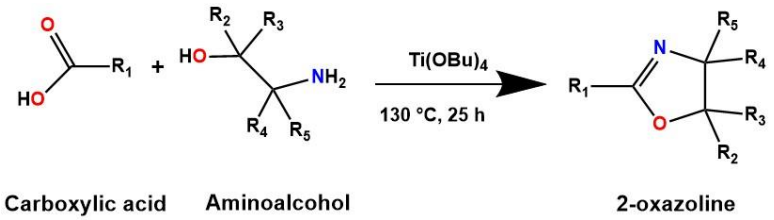

Figure 10: Schematic representation of the synthesis of 2-oxazolines by the Henkel patent.

3.5.3 Synthesis of 2-But-3´-enyl-2-oxazoline according to Hoogenboom

The synthesis protocol[42] is for 2-oxazoline monomers with short side-chains ranging from 1 to 4 carbon atoms in the side-chain. The reactant 2-methyl-2-oxazoline is dropped into a freshly prepared solution of lithium diisopropylamide LDA at a temperature of −78 °C. Subsequently, allyl bromide is added. The reaction mixture is allowed to warm to room temperature, stirred overnight, and afterwards quenched with methanol. Under reduced pressure, all volatiles must evaporated. The crude product has to be washed with water and brine purified by vacuum distillation.

3.5.4 Synthesis of 2-But-3´-enyl-2-oxazoline according to Schlaad

The synthesis of 2-but-3´-enyl-2-oxazoline by the protocol of Schlaad[41] is a three-step synthesis. The starting material is pent-4-enoic acid, which is converted into an active ester in the first step. In the second step,

chloroethylamine hydrochloride is used to convert the active ester into an open-chained *N*-(2-chloroethyl)-pent-4-enamide. The last step is the ring-closing to yield 2-but-3´-enyl-2-oxazoline with potassium hydroxide in methanol (Figure 11). The disadvantages of this synthesis are long reaction times, high amounts of halogenated solvent and low yields.

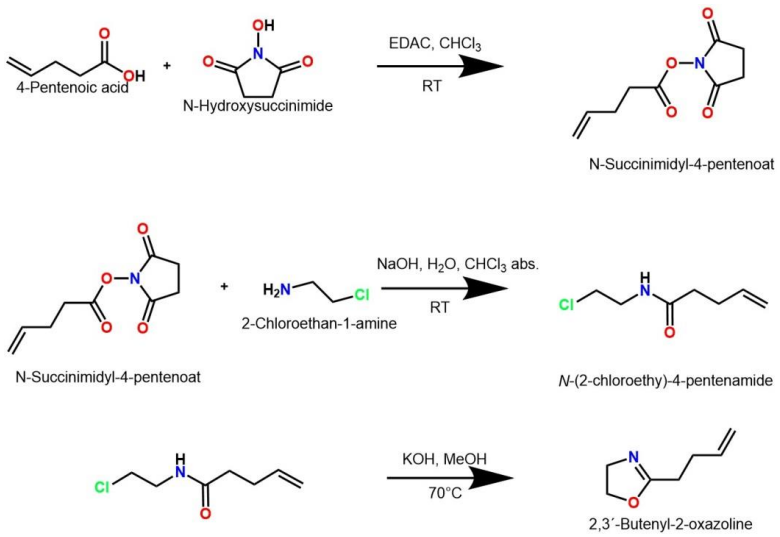

Figure 11: Schematic representation of the synthesis of 2-oxazolines according to Schlaad.

3.6 Microwave-Assisted Polymerizations

Poly(2-oxazoline)s are a polymer class that was found by four different groups at a similar time between 1966 and 1967.[43–46] At that time, the synthesis of poly(2-oxazoline)s was challenging and this polymer class lost wide-spread attention in the 1980's. In recent years, the polymer class was awaken from hibernation, thanks to the innovations in microwave reactors designed for chemical syntheses.[47]

The polymerization of poly(2-oxazoline)s is a cationic ring-opening polymerization, which can be initiated by methyl tosylate (Figure 12).[48] One advantage of poly(2-oxazoline)s is the wide variety of monomers. The broad spectrum of monomers with different functional groups and hydrophobic/hydrophilic properties allows the specific adjustment of

material properties in the copolymers.[49] The poly(2-oxazoline)s employing olefinic moieties at the side chains can be used in negative photoresists, after crosslinking with a dithiol under UV-mediated thiol-ene reactions to yield three-dimensional polymer networks.[14]

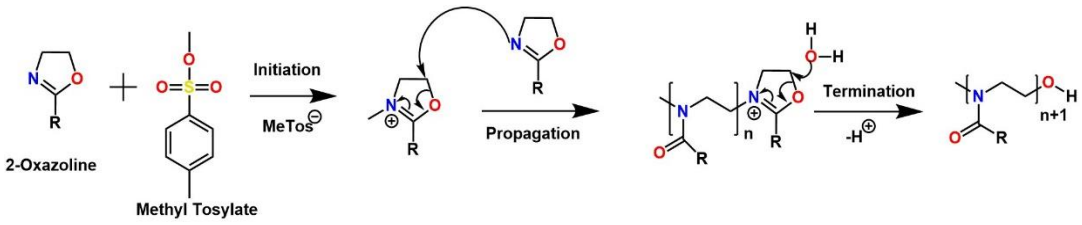

Figure 12: Reaction mechanism of the cationic ring-opening polymerization of oxazolines, with methyl tosylate as initiator.

Due to the pseudo-living character of the cationic ring-opening polymerization of numerous 2-oxazolines, different types of 2-oxazoline-based copolymers such as homopolymers, statistical copolymers, gradient copolymers, and block copolymers can be synthesized.[50]

3.6.1 Homopolymerization of 2-Oxazolines

The group of Schubert described the synthesis of poly(2-ethyl-2-oxazoline)s under conventional heating (reflux in acetonitrile at 81 °C),[51] which yields a polymerization degree of 60 within 6 h. At autoclave conditions in a microwave reactor (190 °C and a pressure of 11 bar), the reaction time was decreased to less than 1 min. Hence, the reaction time was accelerated by a factor of 350. This study has shown that the reaction speed under autoclave conditions is no longer limited by the boiling point of the solvent. The pseudo-living polymerization character was maintained at higher temperatures and lower solvent concentrations.[51] More detailed studies about the influence of the side-chain to the mechanical and thermal properties of poly(2-oxazline)s were published.[52] Recently,

researchers investigated alternatives to the most common initiator methyl tosylate such as alkyl nosylates and alkyl triflates. They are favourable over halide initiators, as halide initiators not only propagate cationic but also covalent species.[53] Wiesbrock et. al. investigated the π-electron delocalization along the N-C-O segment, which confirmed the generally accepted thought that the ring-opening is initiated by a nucleophilic attack at the nitrogen atom.[54]

3.6.2 Block Copolymerisations of 2-Oxazoline Monomers

In the year 2005, Schubert and colleagues synthesized a library of diblock copolymers and chain-extended homopolymers of the monomers 2-methyl-2-oxazoline MeOx, 2-ethyl-2-oxazoline EtOx, 2-phenyl-2-oxazoline PhOx, and 2-nonyl-2-oxazoline NonOx. The deblock copolymers had 50 repetition units in each block and were synthesized under non-conductive (microwave-assisted) heating.[48] Further investigations addressed the glass-transition temperature T_g and thermal stability. For homo- and copoly (2-oxazoline)s, T_gs in the range between 57 and 107 °C were found; for copolymers with more than 50% of NonOx, no T_g could be found. Thermogravimetric analysis revealed thermal stability for all poly(2-oxazoline)s up to 300 °C.[55] Another study dealt with a 30-membered library of triblock copoly(2-oxazoline)s composed of MeOx, EtOx, NonOx and PhOx. The triblock copoly(2-oxazoline)s had 100 repetition units (33 per block). Detailed analyses revealed that copoly(2-oxazoline)s with a hydrophobic part in the centre yielded smaller micelles.[56]

3.6.3 Statistical Copolymerisations

Schubert and colleagues reported EtOx/NonOx-based copoly(2-oxazoline)s with different molecular architectures.[57] The surface energy, kinetics and molar mass dispersity for random and block copolymers were

compared. Contact-angle measurements of the polymer films disclosed abundant surface presence of the alkyl side-chains of the NonOx repetition units, inducing a decrease of the surface energy in the diblock copoly(2-oxazoline)s.[58] An analogous decrease of the decrease could *not* be observed in the statistical copoly(2-oxazline)s that contained NonOx. Further comparisons of block copoly(2-oxazoline)s and random copoly(2-oxazoline)s revealed a lower degree of crystallinity and lower T_g (resulting in lower E modules), higher mechanical energy dissipation (constituting viscoelastic properties), and greater creep compliance for the latter named. The mobility of the side-chain has a strong influence on the surface energies.[59]

Schubert and co-workers also synthesized homopolymers and amorphous copoly(2-oxazoline) from EtOx and 2-(3'-ethylheptyl)-2-oxazoline EHOx. The surface and thermal properties of the copolymers with EtOx:EHOx ratios ranging from 100/0 to 0/100 were evaluated. A linear dependency between the amount of EHOx in the copolymers and the T_g was identified. With an increasing amount of EHOx in the copolymers, a decrease of the surface energy was observed. A further study correlated the branching position with the thermal behaviour as well as the elastic modulus; it was shown that the branching position had a strong effect on the side chain mobility.[59,60]

3.7 Polymeranalogous Reactions of Poly(2-oxazoline)s

A large number of polymeranalogous reactions exists in order to modify copoly(2-oxazoline)s and/or to add additional functionalities to the side-chains of the copoly(2-oxazoline)s . This chapter will give an overview of three specific post-polymerization reactions, namely an overview of click-chemistry and crosslinking reactions as well as the hydrolyses of copoly(2-oxazoline)s. Photolithography and antireflective coatings based on copoly(2-oxazoline)s are highlighted in dedicated chapters.

3.7.1 Click-Chemistry

Click-chemistry is a term that summarizes various methods that follow the same reaction criteria. Such reactions yield no dangerous side-products, exhibit high selectivity and nearly quantitative conversion. This principle originated from organic chemistry, where Kolb and Sharpless investigated the copper(I)-mediated azide-alkyne 1,3-dipolar cycloaddition.[15] According to Hoyle, click reactions are characterized by specific attributes, namely regio- and stereospecific reactions, high yields without side-reactions, mild reaction conditions with or without solvent or water as solvent whenever possible, orthogonality to other organic synthesis reactions, insensitivity to moisture and oxygen, and the availability of a wide variety of starting compounds.

In click-chemistry, there are two common thiol reactions, the radical thiol-ene-addition to electron-poor and electron-rich carbon-carbon bonds as well as the catalyzed thiol-Michael-addition to electron poor carbon-carbon bonds. Due to the mild conditions, high efficiency, and wide variety, the thiol-ene chemistry is often used for the crosslinking of polymers. The radical thiol-ene reaction be initiated thermally or by means of UV irradiation.[61] For the UV-induced initiation, only a small amount of photoinitiator PI is necessary, which is homolytically cleaved into two radical fragments (Figure 13). These radicals interact with the thiol compound and form thiyl radicals. The thiyl radicals interact with carbon-carbon double bonds yielding thiol ethers. An advantage of the thiol-ene cycle (Figure 14) is that there are only minor side-reactions.[62]

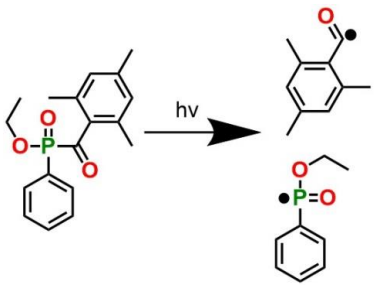

Figure 13: Photo-initiated fragmentation of the PI Irgacure® TPO-L.

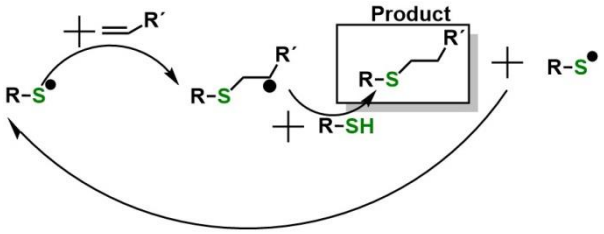

Figure 14: Reaction scheme of thiol-ene reaction, highlighting the thiol-thiyl cycle.

Gress, Völkel and Schlaad published the functionalization of olefinic side-chain of poly(2-oxazoline)s by thiol-ene-reactions.[41] They used poly[2-(but-3'-enyl)-2-oxazoline] and methyl-3-mercaptopropionate for this reaction. In the year 2010, Schubert and co-workers investigated the cellular uptake of copoly(2-oxazoline)-based nanoparticles. The nanoparticle size ranged from 200 to 600 nm, and was varied by the concentration of the monomers EtOx and 2-dec-9´-enyl-2-oxazoline $Dc^{=}Ox$. They used the thiol-ene click chemistry to functionalize the repetition units of $Dc^{=}Ox$ with fluorescein.[63]

3.7.2 Crosslinked Copoly(2-oxazoline)s

By means of UV-induced thiol-ene reactions involving the unsaturated double bonds of copoly(2-oxazoline)s, it is possible to generate three-dimensional frameworks. Hence, copoly(2-oxazoline)s can be employed in negative photoresists (Chapter 3.7.5). The swelling capacity of crosslinked copoly(2-oxazoline)s networks has been evaluated in different studies.[64–67] The copoly(2-oxazoline)-based hydrogels were synthesized and crosslinked; their swelling capacity in different solvents (e.g. dichloromethane, ethanol, water) was investigated. Further studies addressed the application of poly(2-oxazoline)-based hydrogels in the field of medical and medicinal technology, benefiting from the biodegradability of this polymer class.[68] One approach was the bonding of peptides to the hydrogels in order to promote their adhesion cancer cells. Another study by Wiesbrock et al. investigated the (enzymatic)

degradation of hydrogels at different pH values.[65] A new application of crosslinked copoly(2-oxazoline)s was investigated by Wiesbrock and co-workers. The electrical conductivity and permittivity of copoly(2-oxazoline)s, namely pNonOx$_{80}$-*stat*-pDc$^{=}$Ox$_{20}$ and pDc$^{=}$Ox$_{100}$, was explored. Notably, both types of monomers were synthesized from renewable resources. The two copoly(2-oxazline)s were crosslinked by the polymeranalogous UV-induced thiol-ene reaction involving the carbon-carbon double bond of the Dc$^{=}$Ox repetition units. As crosslinker, multifunctional thiols were used. The study showed the relative permittivity and the electric conductivity of the copoly(2-oxazoline)s were quasi-identical to those of polyamides, which renders the poly(2-oxazoline)s potential candidates for high-voltage insulators.[69]

3.7.3 Hydrolysis

Litt and co-workers evaluated the alkaline and acidic hydrolysis of various block copoly(2-oxazoline)s; a kinetic analysis showed second-order reaction kinetics of the acidic hydrolysis.[70] Menzel and colleagues investigated the alkaline hydrolysis of poly(2-methyl-2-oxazoline) and found that the gelation concentration decreased with increasing polymerization degree. [71] Another study investigated the potential toxicity of partially hydrolyzed poly(2-oxazoline)s. Poly(2-methyl-2-oxazoline) was hydrolyzed with 5.8 M hydrochloric acid. Due to the first-order kinetics, the degree of hydrolysis correlated with the reaction time. After 6 h hydrolysis at 37 °C and a pH value of 1.2, less than 0.2% of the copoly(2-oxazoline) was hydrolyzed.[72]

3.7.4 Photolithography

The semiconductor and computer industry have vivid interest in polymer-based photoresists. Because of the high resolution of photoresists,

computer chips can be manufactured in continuously decreased feature sizes. There are two types of photoresists, those that mirror the positive image and those that reproduce the negative image of a used mask (Figure 15). The illuminated parts of the photoresist undergo photochemical reactions, by which the solubility is influenced. For negative resists, the solubility of the illuminated parts decreases; for positive resists, the illuminated parts become more soluble.

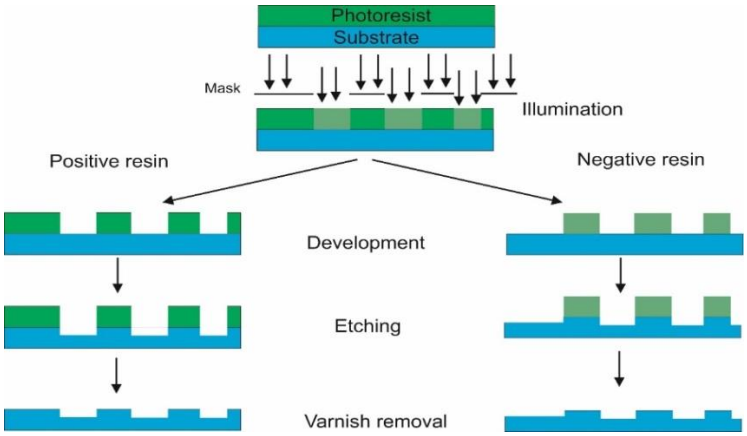

Figure 15: Schematic diagram of the operation principle of positive (left hand-side) and negative (right hand-side) photoresists.

3.7.5 Poly(2-oxazoline)s as Photoresists and Antireflective Coatings

In the year 1999, Havard and co-workers investigated poly(2-isopropyl-2-oxazoline) and poly(2-isoporpyl-oxazoline-*co*-styrene) as two component photoresists.[73] Films with heights of 0.7 µm were spin-coated; the smallest feature size was 1.5 µm. Wiesbrock and co-workers investigated photoresists based on the copoly(2-oxazoline)s pPhOx$_{80}$-*stat*-pDc$^{=}$Ox$_{20}$ and pEtOx$_{80}$-*stat*-pBu$^{=}$Ox$_{20}$. The photoresist films were 6 and 10 µm high; the smallest feature size was 2 µm. Both polymers had double bonds in their side-chains, which can react with a thiol in UV-induced thiol-ene reactions, yielding a crosslinked polymer if oligofunctional thiols are used (Figure 16).[14] It is possible to develop pEtOx$_{80}$-*stat*-pBu$^{=}$Ox$_{20}$ with water.

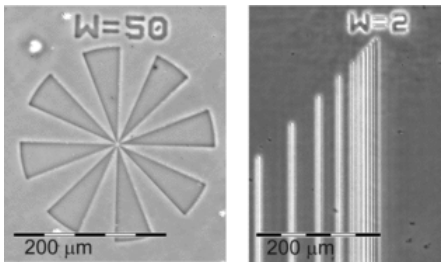

Figure 16: Phase contrast image of crosslinked $pEtOx_{80}$-*stat*-$pBu^{=}Ox_{20}$ after UV irradiation and development.[14]

A further study evaluated the environmentally friendly synthesis of the photoresist $pNonOx_{80}$-*stat*-$pDec^{=}Ox_{20}$. The reactants for the monomer synthesis can be derived from renewable resources, namely coconut oil and castor oil. As ionic liquid for the microwave-assisted copolymerization, *n*-hexyl methylimidazolium tetrafluoroborate was used. The photoresist had a resolution of 1 µm.[13] Wiesbrock et al. also investigated antireflective coatings based on copoly(2-oxazoline)s. EtOx, $Dc^{=}Ox$, $Bu^{=}Ox$ and $Pen^{=}Ox$ (2-pent-4′-inyl-2-oxazoline) were copolymerized to yield $pEtOx_{45}$-*stat*-$pDc^{=}Ox_{20}$-*stat*-$pPen^{=}Ox_{35}$ and $pEtOx_a$-*stat*-$pBu^{=}Ox_b$-*stat*-$Pen^{=}Ox_c$ (a:b:c = 70:15:15, 60:15:15). The copolymers were functionalized with anthracene chromophores by the Huisgen 1,3-cycloaddition under mild conditions. This functionalisation lowered the amplitude of the swing-curve significantly (Figure 17).[74]

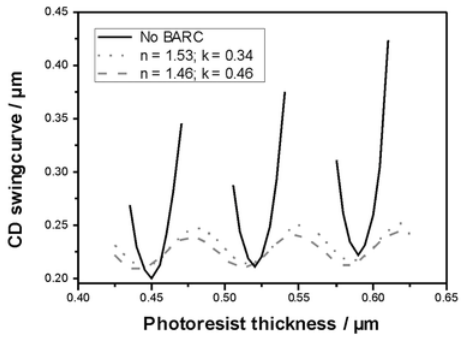

Figure 17*:* Sinoidal-shaped swing-curves of a stack of the photoresist M91Y and substrate (solid line) or photoresist M91Y and a stack of BARC and substrate (dotted and dashed line).[74]

4. Novel Results

The monomers chosen for this study were 2-dec-9'-enyl-2-oxazoline Dc$^{=}$Ox (bearing a double bond in the side-chain) and 2-nonyl-2-oxazoline NonOx. Both monomers can be synthesized from renewable resources. Due to the long non-polar side-chains of NonOx and Dc$^{=}$Ox, hydrophilic copoly(2-oxazoline)s will be obtained with low water uptake. Three-dimensional networks can be generated from copoly(2-oxazoline)s containing repetition units of Dc$^{=}$Ox via the thiol-ene reaction with multifunctional thiols, enabling the inclusion of nanofillers in such polymeranalogous crosslinking reactions. These crosslinked networks were characterized in physico-chemical as well as dielectric fashion, aiming at the quantification of their applicability as high-voltage insulators.

4.1 Synthesis of the Monomers NonOx and Dc$^{=}$Ox

NonOx was synthesized following the Henkel patent[39] (Chapter 3.5.2) from the reaction of decanoic acid with ethanolamine, with Ti(IV)butoxide as catalyst; Dc$^{=}$Ox was synthesized as well according to the Henkel patent from the fatty acid 10-undecenoic acid (Figure 18).

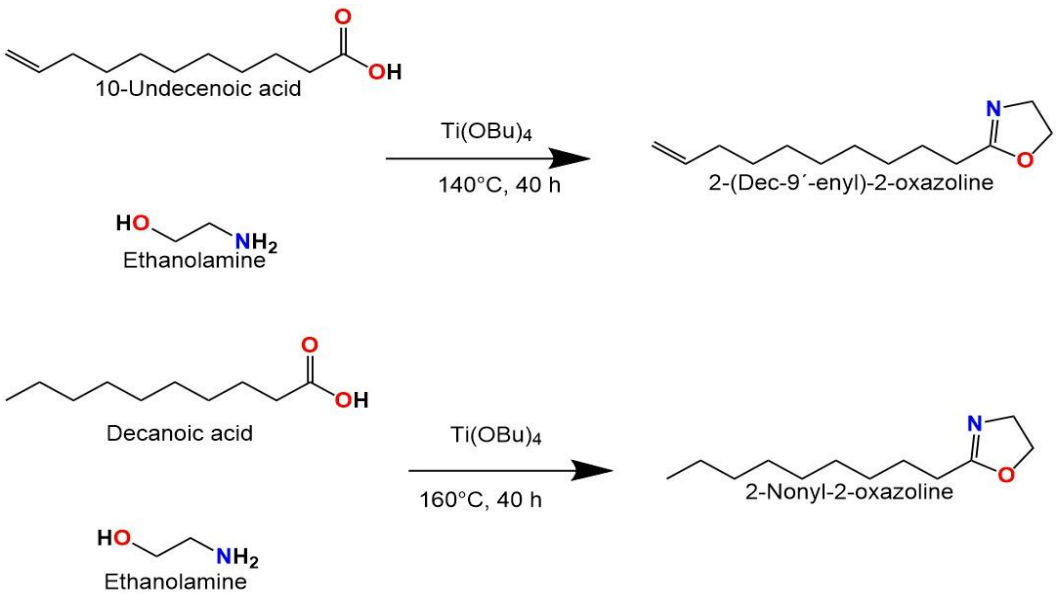

Figure 18: Synthesis of Dc$^{=}$Ox (top) and NonOx (bottom).

Both monomers, NonOx as well as Dc$^{=}$Ox, could be recovered from the reaction mixture and purified by vacuum distillation. The ^{1}H-NMR spectra (Figures 19 and 20) reveal the purity of the two compounds.

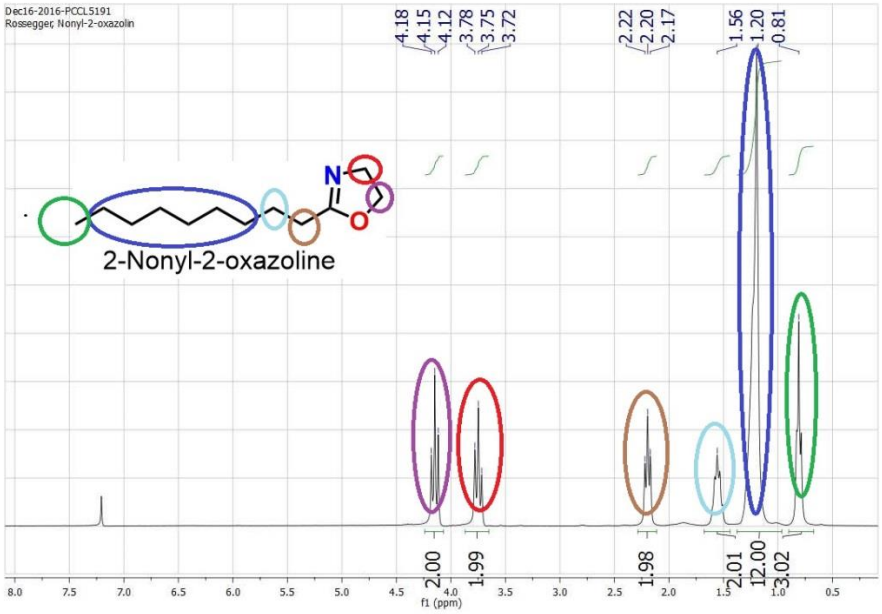

Figure 19: ^{1}H-NMR spectrum of 2-nonyl-2-oxazoline NonOx.

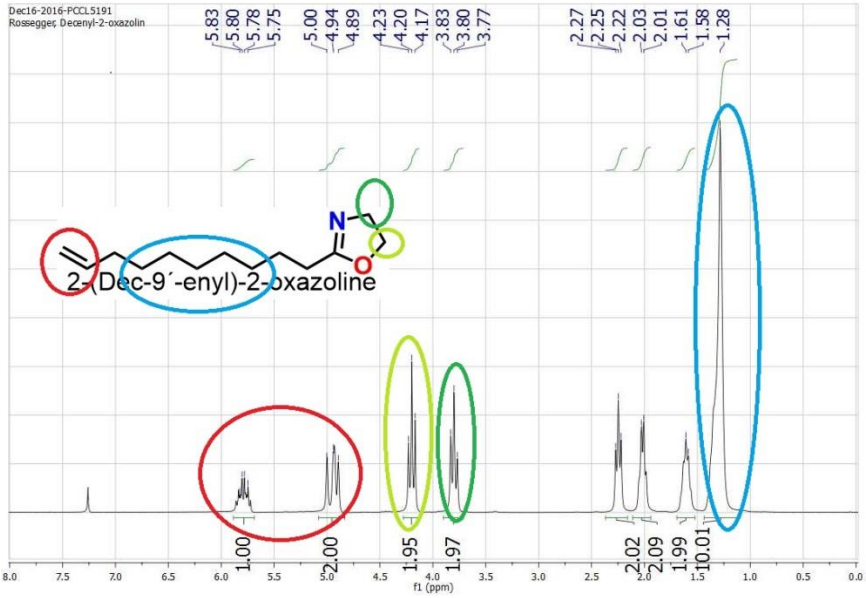

Figure 20: ^{1}H-NMR spectrum of 2-dec-9´-enyl-2-oxazoline Dc$^{=}$Ox.

4.2 Microwave-Assisted Copolymerization: Synthesis of pNonOx$_{75}$-*stat*-pDc$^{=}$Ox$_{25}$

Via the microwave-assisted, pseudo-living cationic ring-opening polymerisation of NonOx and Dc$^{=}$Ox, the copolymer of the targeted composition pNonOx$_{75}$-*stat*-pDc$^{=}$Ox$_{25}$ can be synthesized in straight-forward manner. For the synthesis of 10 g of the copoly(2-oxazoline) pNonOx$_{75}$-*stat*-pDc$^{=}$Ox$_{25}$, 7.39 g NonOx, 2.61 g Dc$^{=}$Ox, and 92.3 mg methyl tosylate were dissolved in 10 mL of acetonitrile and placed in a 20 mL microwave vial. The polymerization was performed under autoclave conditions in a Biotage microwave reactor at 140 °C and a pressure of 4 bar for 2.5 h.

After removal of the solvent, pNonOx$_{75}$-*stat*-Dc$^{=}$Ox$_{25}$ was dried under reduced pressure (< 2 mbar) for 5 h. The ^{1}H-NMR spectrum of the copolymer (Figure 21) reveals the absence of any residual un-recated monomers. Furthermore, it enables verifaction of the 75:25 ratio of the repetition units: Assuming that the polymer back-bone has 100·4 = 400 hydrogen atoms, the methyl end group of the NonOx side-chain shows 75·3 = 225 hydrogen atoms, and the double bond at the end of the Dc$^{=}$Ox sidechain has 25·3 = 75 hydrogen atoms.

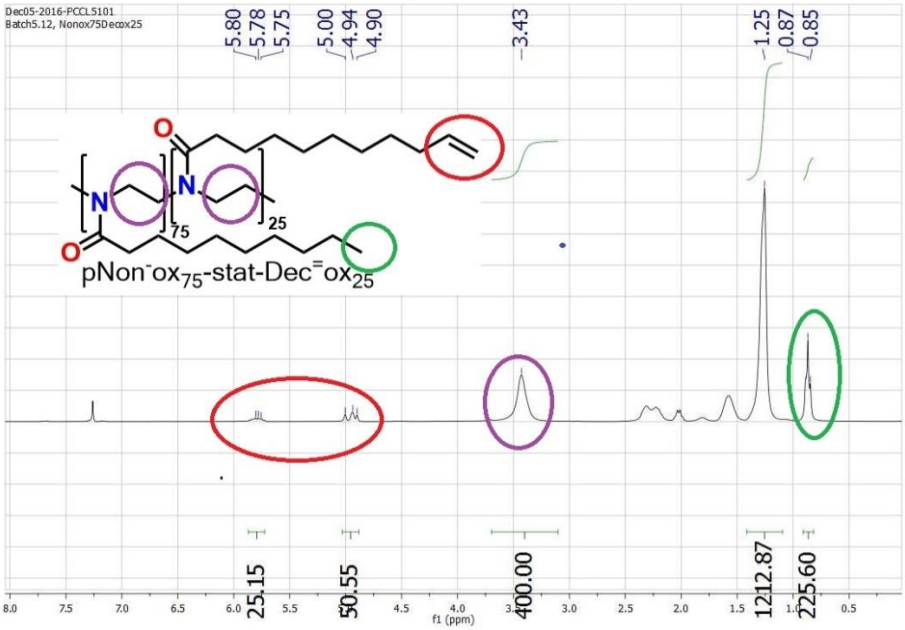

Figure 21: ^{1}H-NMR spectrum of pNonox$_{75}$-*stat*-pDc=Ox$_{25}$.

4.3 IR Spectroscopy of the Nanoparticles

The nanoparticles used for the production of poly(2-oxazoline)-based nanocomposites needed to fulfil certain requirements such as electric insulation, high thermal conductivity and commercial availability. Nanoparticles that meet these requirements are (native) silica, (native) alumina, (native and modified) boron nitride, and (modified) nanodiamonds (Table 1).

Table 1: Particle sizes of the nanoparticles.

Nanoparticle	Size [nm]
Al_2O_3	13
SiO_2	5-15
BN	135
Modified BN	339
Modified ND	132

For the characterization of the nanoparticles, IR spectra were recorded (Figures 22 to 26). With special respect to characterizing the surface of the nanoparticles, ATR (attenuated total reflection) measurements were performed. The region which was investigated in detailed fashion is between 2900 and 3000 cm^{-1} as this is the region indicative of hydroxy groups; hydroxy groups on the surface of the nanoparticles are likely to interact with the copoly(2-oxazoline)-based polymer matrix. None of the un-modified nanoparticles, namely silica, alumina, and hBN, show significant absorbance in this region; in fact, the IR spectra perfectly correspond with the literature data of the compounds. The modified nanoparticles, namely modified nanodiamonds and modified hBN, show a comparably high level of absorption in the region around 3000 cm^{-1}, indicative of surficial hydroxy groups.

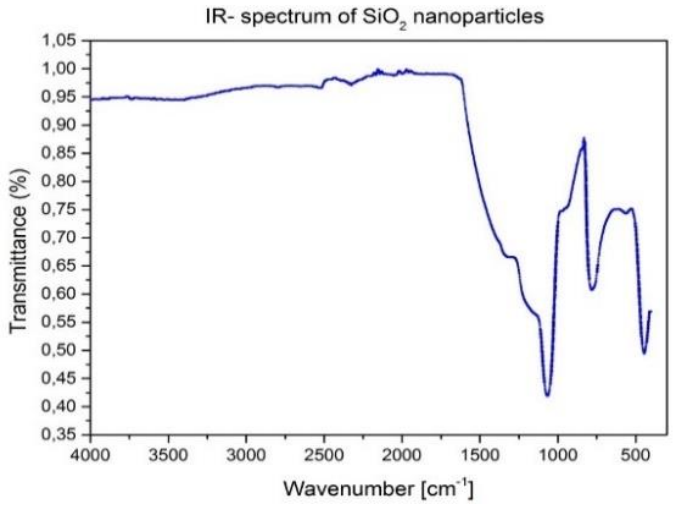

Figure 22: IR spectrum of un-modified SiO_2 nanoparticles.

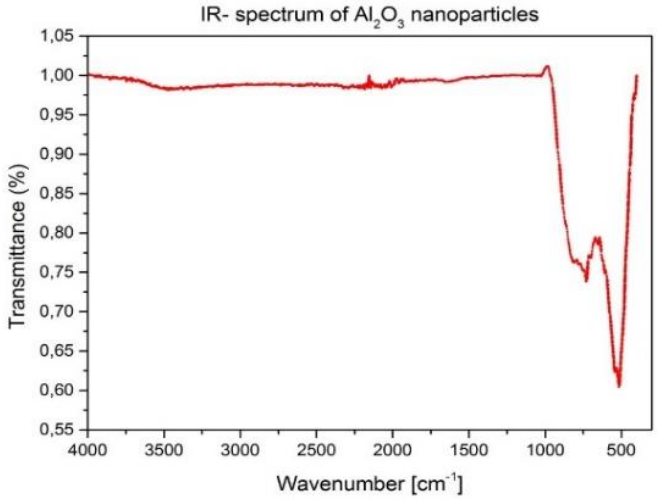

Figure 23: IR spectrum of un-modified Al_2O_3 nanoparticles.

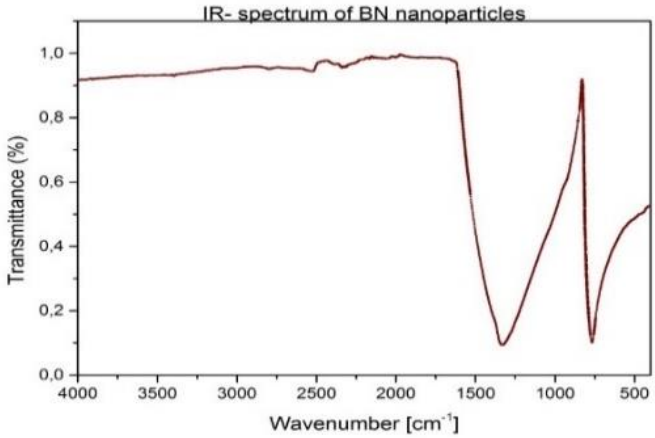

Figure 24: IR spectrum of un-modified hBN nanoparticles**.**

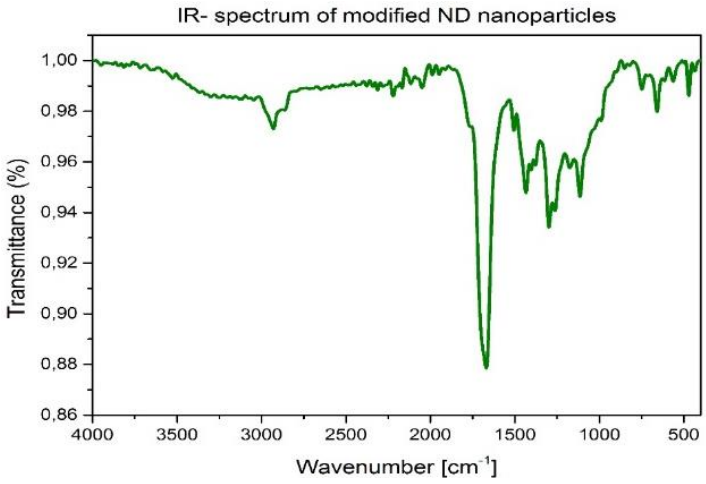

Figure 25: IR spectrum of modified ND nanoparticles.

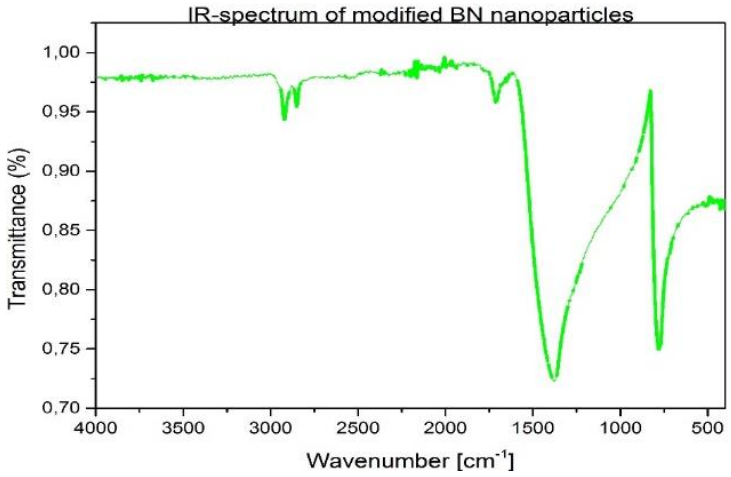

Figure 26: IR spectrum of modified hBN nanoparticles.

4.4 Manufacturing of the Crosslinked Copolymer and the Nanocomposites

Dried samples of the copolymer pNonOx$_{75}$-*stat*-pDc$^{=}$Ox$_{25}$ were fine-crushed in a mortar, and the crosslinker, namely the bifunctional thiol GDMA (Figure 27), one type of nanoparticles (10 wt.-%), and the photoinitiator Lucirin TPO-L were added and mixed vigorously. The mixture was filled into a circular steel template and put into a panel press

at 180 °C and 35 bar pressure, for 15 min (break down voltage and permittivity measurements) and 30 min (for the preparation of the thermal conductivity specimen), respectively. The specimens were subsequently taken out of the template and illuminated (2 minutes, 5000 mW/cm², 10 cm).

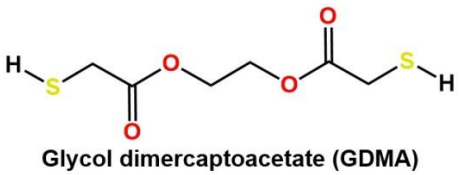

Figure 27: Bifunctional crosslinker for the UV-induced thiol-ene reaction.

For all analyses, 6 types of specimen were prepared:

- unfilled pNonOx$_{75}$-*stat*-pDc$^{=}$Ox$_{25}$ copolymer
- pNonOx$_{75}$-*stat*-pDc$^{=}$Ox$_{25}$ with 10 wt.-% of unmodified SiO_2
- pNonOx$_{75}$-*stat*-pDc$^{=}$Ox$_{25}$ with 10 wt.-% of unmodified Al_2O_3
- pNonOx$_{75}$-*stat*-pDc$^{=}$Ox$_{25}$ with 10 wt.-% of unmodified hBN
- pNonOx$_{75}$-*stat*-pDc$^{=}$Ox$_{25}$ with 10 wt.-% of modified hBN
- pNonOx$_{75}$-*stat*-pDc$^{=}$Ox$_{25}$ with 10 wt.-% of modified nanodiamonds.

The specimen geometry was adjusted to each measurement set up as described in chapter 4.5.

4.5 Differential Scanning Calorimetry

4.5.1 Measurement Protocol

Differential scanning calorimetry (DSC) was used to determine the glass-transition temperature T_g, the melting point T_m and changes in the crystalline phase of the polymers.[75] With a heat rate of 10 K/min, two

pans were heated in one measurement chamber. One pan was filled with the specimen, and a second (reference) pan was empty or filled with a reference substance. Due to the different contents in the pans, the up-taken temperature rate will differ for the two pans because of physical changes such as melting, change of morphology or degradation. The different heat uptake was recorded, yielding the correlation of heat and temperature.

The heat needed to increase the temperature by 1 K is called heat capacity C_p. For the calculation of C_p, which has the unit J/K, the heat flow and heating rate are needed. The heat flow is calculated by dividing heat by time (Equation 2). For calculating the heating rate, the temperature change is divided by time (Equation 3). By deviating the heat flow by the heating rate, the heat capacity can by calculated (Equation 4).

$$\text{Heat flow} = \frac{\text{heat}}{\text{time}} = \frac{q}{t} \tag{2}$$

$$\text{Heating rate} = \frac{\Delta T}{t} \tag{3}$$

$$\text{Heat capacity } C_p = \frac{\frac{q}{t}}{\frac{\Delta T}{t}} = \frac{q}{\Delta T} \tag{4}$$

The glass-transition temperature T_g is the temperature, at which the mobility of the polymer chains alters: The mechanical properties change above the glass-transition temperature from brittle material to elastic. The heat capacity increases above T_g, which is a result of the change in chain mobility. At a certain temperature, the chains have enough energy to form ordered arrangements, which leads to crystallisation. Due to the exothermic process of crystallisation, heat is transferred to the environment from the pan. The specimen pan has a lower heat uptake than the reference pan, therefore a decrease in the heat flow is recorded. The lowest point of the peak is the so-called crystallisation temperature T_c. At the melting temperature T_m, the polymer chains can move freely and loose the ordered arrangement. During the melting of the polymer, heat is absorbed (endothermic process), and, despite constant heating, the

temperature does not increase during the melting process. After complete melting of the polymer, the temperature increases again.[75]

4.5.2 Measurement of the Nanocomposites

The DSC measurements were performed in the temperature range from 30 to 200 °C. For the calculations, only the *first* heating circle was considered (Figure 28). The results of the DSC measurement indicate an endothermic peak between 40 and 60 °C, followed by an exothermic region from 70 to 130 °C. The absence or presence of nanofillers was found not to alter the crystallization behaviour of the polymer (matrix).

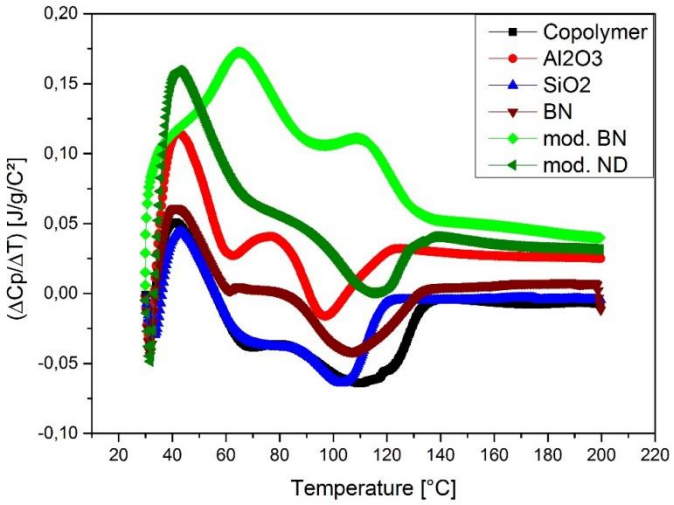

Figure 28: DSC measurement of all nanocomposites.

4.6 Electrical Breakdown Strength

4.6.1 Measurement Protocol

The dielectric breakdown is the failure of dielectrics under electrical stress, with every electric breakdown causing a permanent damage on the solid dielectric. Dielectric strength is the maximum amount of an electric field that can be applied to an insulation material, without causing electric

breakdown. The dielectric strength is strongly related to the thickness of the specimen, due to its definition as the ratio between the breakdown voltage and the distance between the electrodes, usually measured under standard protocol, ASTM D 149-97a at 60Hz.[76] The specimen is placed between two electrodes in mineral oil (Figure 29). The upper electrode is the high-voltage electrode, and the lower electrode is the earth electrode. The specimens were placed for 4 days in a vacuum oven at 100 °C prior to the measurements. From every type of nanocomposite, 5 specimens were measured.

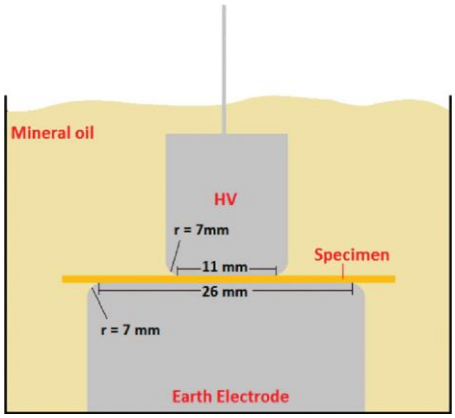

Figure 29: Set-up for the quantification of the breakdown strength.

4.6.2 AC Breakdown Measurements

The voltage was increased by 1 kV/s during the AC breakdown measurements. All specimens, the copolymer as well as the nanocomposites, were all found to be stable up to the range of 45 kV·mm^{-1} (AC; Figure 30). The breakdown strength comprised a range from 43.8 (copolymer with 10 wt.-% of modified hBN) to 50.63 kV·mm^{-1} (copolymer with 10 wt.-% of ND). Compared to commercially used epoxy resins such as CY 1300 that have a breakdown strength of approx. 60 kV·mm^{-1}[76], the results of the copoly(2-oxazoline)-based nanocomposites are in the same range of the AC breakdown strength.

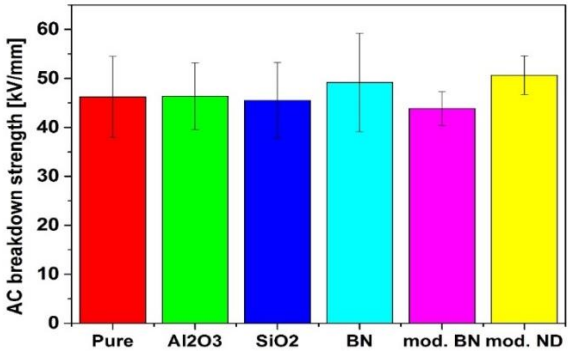

Figure 30: AC breakdown strength of copolymer and nanocomposites.

4.6.3 DC Breakdown Measurements

The increasing speed for the DC electric breakdown measurements was 2 KV/s. Unlike the AC measurements, the DC breakdown strength of the copoly(2-oxazoline) nanocomposites was found to vary with the addition of nanoparticles (Figure 31): Samples with 10 wt.-% of SiO_2 had an average DC breakdown strength of approx. 100 $kV \cdot mm^{-1}$ (the highest value of this study), while the pure copoly(2-oxazoline) was stable only up to approx. 60 $kV \cdot mm^{-1}$. Overall, the addition of nanoparticles had a positive influence on the DC breakdown strength, compared to the pure copoly(2-oxazoline). All additives (except for alumina Al_2O_3) increased the AC breakdown strength of the corresponding samples. The DC breakdown strength of pure epoxy resins such as CY231, a bisphenol A-based resin, is in the range of 150 $kV \cdot mm^{-1}$[77].

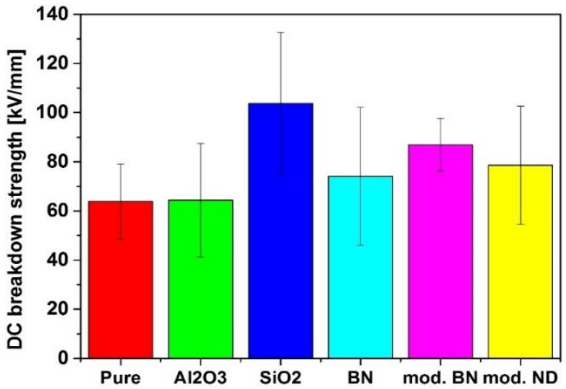

Figure 31: DC breakdown strength of the copolymer and nanocomposites.

4.7 Dielectric Polarization and Permittivity

4.7.1 Polarisation mechanism

If an external electric field E is applied to a material, the electric field forces the charges in the material to relocate. Positive and negative charges are shifted from each other, and a dipole will be formed. The polarisation P is the sum of dipoles per volume in the material. There is a distinction between four different polarisation mechanisms, namely electrical, ionic, orientation and space charge.

4.7.2 Relative permittivity

In a parallel capacitor, the dielectric capacitance D of free space (with the permittivity ε_0=8.854·10^{-12} F·m^{-1}), is increased by the dipole polarisation P (Equation 5). A proportional correlation exists between the dielectric polarisation P in free space and the applied electric field E, with the so-called electrical susceptibility χ_e as factor, which can be calculated from the relative permittivity ε_r (Equation 6), yielding the correlation between D and P (Equation 7). Hence, the relative permittivity indicates the relative charge storage capability of dielectrics compared to the relative charge storage capability of free space.[78]

$$D = \varepsilon_0 \cdot E + P \tag{5}$$

$$P = \chi_e \cdot \varepsilon_0 \cdot E \quad \text{with} \quad \chi_e = \varepsilon_r - 1 \tag{6}$$

$$D = \varepsilon_0 \cdot E + \varepsilon_0 \cdot \chi_e \cdot E = \varepsilon_0 \cdot (1+\chi_e) \cdot E = \varepsilon_0 \cdot \varepsilon_r \cdot E \tag{7}$$

4.7.3 Complex Permittivity and Dielectric Loss

When a constant (DC) electric field is applied, a static permittivity $\varepsilon_\mathbf{r}$ results from the polarisation. When an alternating electric field is applied, different polarisation behaviour of the dielectric occurs, as the electric field switches

the orientation faster than the dielectric can switch its polarisation. Thermal agitations are hindered, e.g. in viscous media by the interaction between adjacent moieties. A phase delay occurs between the applied field and the dielectric. This delay is based on the time in which the dielectric orientates itself to the applied electric field, which renders the delay a frequency-dependent factor. The dielectric loss D is predicted from the imaginary permittivity, which is the loss of energy in a material. Figure 32 shows a general overview between the four polarisation mechanisms real and imaginary permittivity and frequency. The definition of the dissipation factor tan (δ) is the relation between the imaginary permittivity ε'' and the relative permittivity ε' (Equations 8 to 9). Generally, a small value for ε'', indicative of small losses of electrical energy, is preferable in the context of insulating media.[25,79]

$$D = \tan(\delta) = \frac{\varepsilon''}{\varepsilon'} = \frac{\text{energy lost per cycle}}{\text{energy stored per cycle}} \quad (8)$$

$$\varepsilon_r = \frac{\varepsilon}{\varepsilon_0} = \varepsilon_r - i\varepsilon_r'' \quad (9)$$

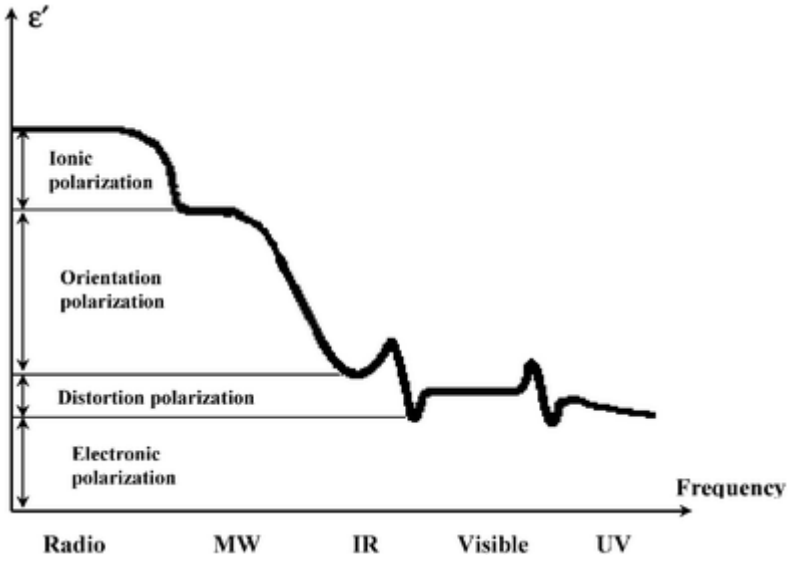

Figure 32: Relation between the polarization mechanisms, the imaginary and relative permittivity and the frequency.[80]

In a recent study, the dielectric properties of copoly(2-oxazoline)s were compared to those of polyamides, polyester and epoxy resins. At 20 °C and 50 Hz (industrial standard), the crosslinked copolymer $pNonOx_{80}$-*stat*-$pDc^{=}Ox_{20}$ exhibited a permittivity of 4.29, which is in the same range as polyamides (3.6-7) or epoxy resins (3.7-4.2). For an ideal dielectric, the loss factor (tan δ) should be as close as possible to zero, because then no/hardly any energy would be stored. On the other hand, the loss factor of an ideal conductor is ∞.[69] Good dielectric materials have a tan (δ) <<1.

4.7.4 Permittivity Measurement Set-up

All specimens were measured at three different temperatures, namely −20, +20 and +60 °C, at a frequency range between 10^{-2} and 10^{7} Hz. In order to compare different materials and insulators, the industrial standard of 20 °C / 50 Hz was used.

4.7.5 Real Part of the Relative Permittivity

The real part of the permittivity increases with decreasing frequencies; in overall summary, this effect is most pronounced for frequencies lower than 100 Hz at 20 and 60 °C, respectively (see Figures 33 to 35). Concomitant with that range of frequencies, the increase of the permittivity can be associated with interfacial polarization, which is highly sensitive to water impurities and irregularities in the material like grain boundaries.[80] Notably, at the lower temperatures of −20 and +20 °C, the unfilled copoly(2-oxazoline)s exhibits a pronounced increase of the permittivity at lower frequencies (so high that the measurements needed to be stopped). Hence, it may be concluded that all nanofillers reduce the (interfacial) polarizability due to particle-matrix interaction.

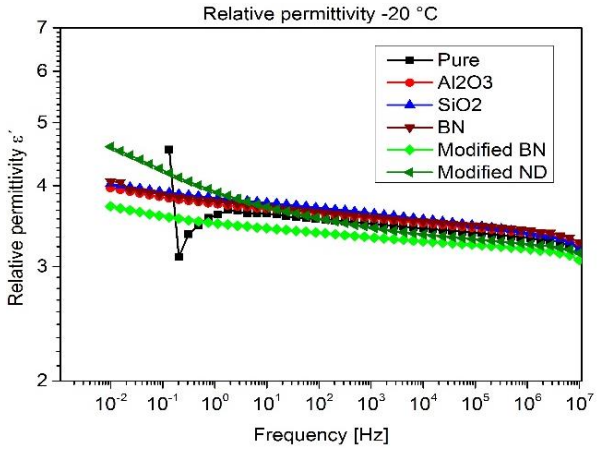

Figure 33: Real part of the permittivity of all nanocomposites at −20 °C.

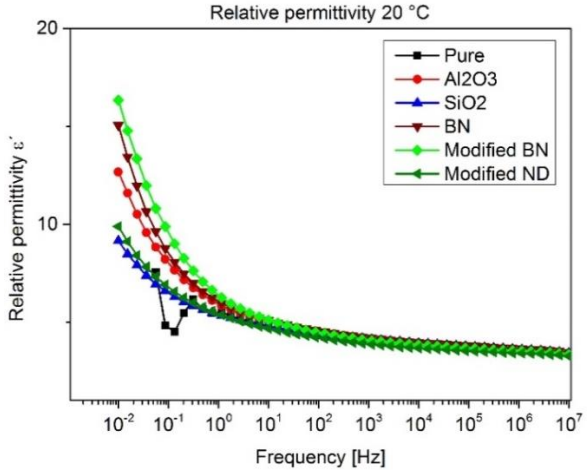

Figure 34: Real part of the permittivity of all nanocomposites at 20 °C.

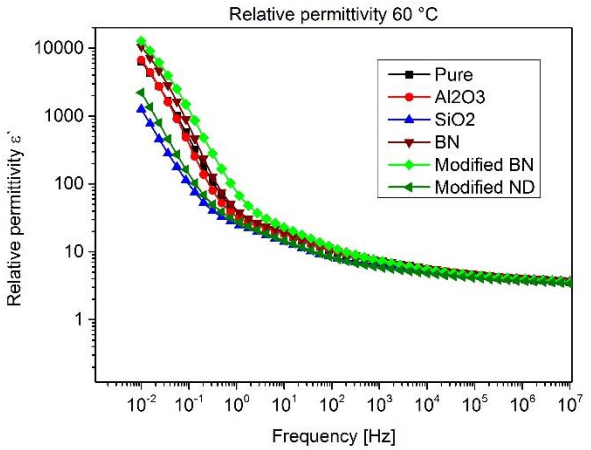

Figure 35: Real part of the permittivity of all nanocomposites at 60 °C.

As expected, the real part of the permittivity increases as well with the temperature at otherwise identical frequencies (Table 2). Despite the exceptional behaviour of the unfilled copolymer, at 20 °C and 50 Hz, the unfilled copolymer as well as all nanocomposites exhibit a permittivity of the narrow range from 4.3 to 4.7.

Table 2: Real part of the relative permittivity at –20, 20 and 60 °C, and 50 Hz.

Specimen ↓ / T →	**-20 °C**	**20 °C**	**60 °C**
Copolymer	3.57	4.42	12.2
10 wt.-% Al_2O_3	3.64	4.69	12.49
10 wt.-% SiO_2	3.72	4.52	9.44
10 wt.-% BN	3.66	4.70	13.19
10 wt.-% mod. BN	3.39	4.61	14.25
10 wt.-% mod. ND	3.60	4.32	9.67

4.7.6 Imaginary Part of the Relative Permittivity

The imaginary permittivity quantifies the energy loss of a material. For an insulator, it should exhibit very low values. Similar to the real part of the permittivity, it was found to increase with increasing temperatures and decreasing frequencies (Figures 36 to 38). The nanocomposites filled with (un-modified) SiO_2, (un-modified) Al_2O_3, and modified boron nitride exhibit the lowest imaginary parts of the permittivity at all temperatures and frequencies. At the lower temperatures of –20 and +20 °C, the unfilled copolymer shows an unrivalled increase of the imaginary part of the permittivity, pronouncedly higher than all nanocomposites. It may be argued that the unfilled copoly(2-oxazoline) (crosslinked with a bifunctional thiol) loses its insulation properties starting from 1000 Hz. At 60 °C, the unfilled copolymer and the nanocomposites show very comparable behaviour.

These observatiions are reproduced by the values for the imaginary part of the permittivity at the industrial standard of 50 Hz (Table 3): While the unfilled copolymer exhibits comparably high values at -20 and +20 °C, all specimens exhibit comparably high values at +60 °C.

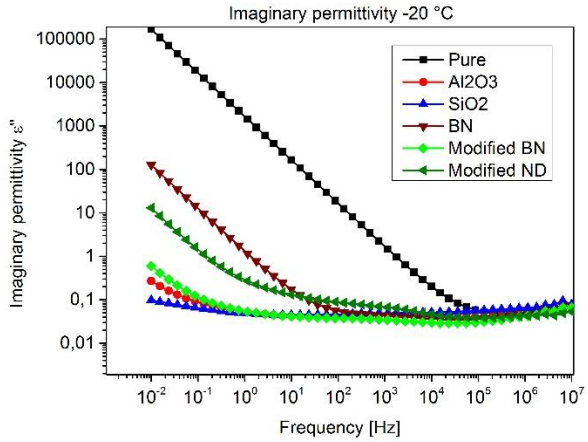

Figure 36: Imaginary part (permittivity) of the nanocomposites at –20 °C.

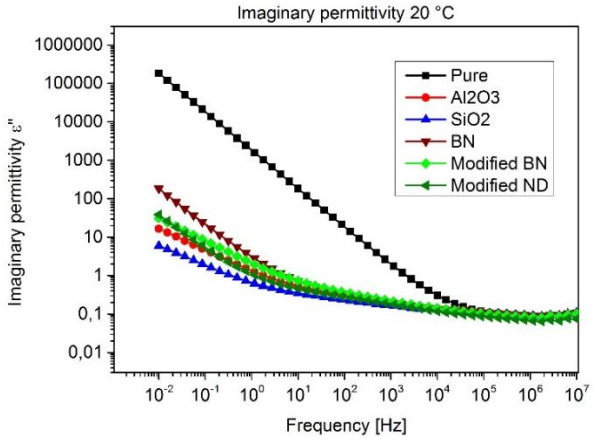

Figure 37: Imaginary part (permittivity) of the nanocomposites at 20 °C.

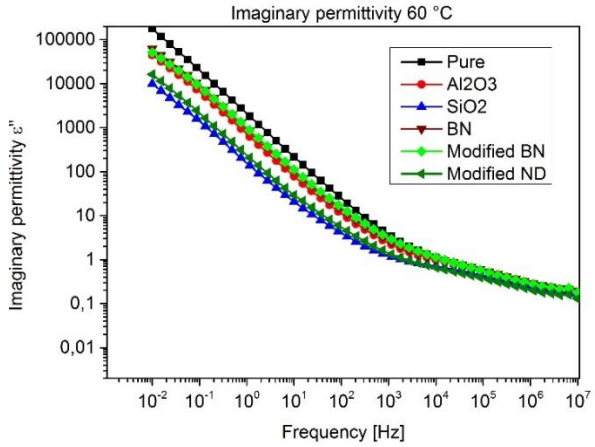

Figure 38: Imaginary part (permittivity) of the nanocomposites at 60 °C.

Table 3: Imaginary part of the permittivity of the nanocomposites at –20, 20 and 60 °C, respectively, and 50 Hz.

Specimen ↓ / T →	–20 °C	20 °C	60 °C
Copolymer	33.49	37.92	46.37
10 wt.-% Al_2O_3	0.04	0.26	19.64
10 wt.-% SiO_2	0.05	0.36	6.36
10 wt.-% BN	0.07	0.4	25.18
10 wt.-% mod. BN	0.04	0.44	27.78
10 wt.-% mod. ND	0.1	0.31	8.71

4.7.7 Dielectric Loss

The definition of the dissipation factor tan (δ) is the relation between the imaginary permittivity ε″ and the relative permittivity ε′ (Equations 8 to 9). Hence, for insulators, the criterion of tan (δ) << 1 must be fulfilled. In general, the loss factor increases with increasing temperatures and lowered frequencies (Figures 39 to 41). Considering the threshold of 1, all nanocomposites can be considered as insulators at frequencies higher than 1 Hz for temperatures of -20 and +20 °C as well as at frequencies higher than 100 Hz at 60 °C (Table 4). The unfilled copolymer loses its insulation properties [tan (δ) > 1] already at frequencies lower than 10^4 Hz at temperatures of -20 and +20 °C, respectively.

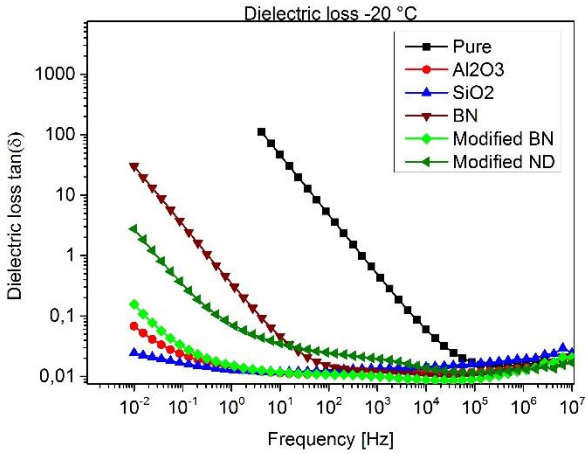

Figure 39: Dielectric loss of the nanocomposites at –20 °C.

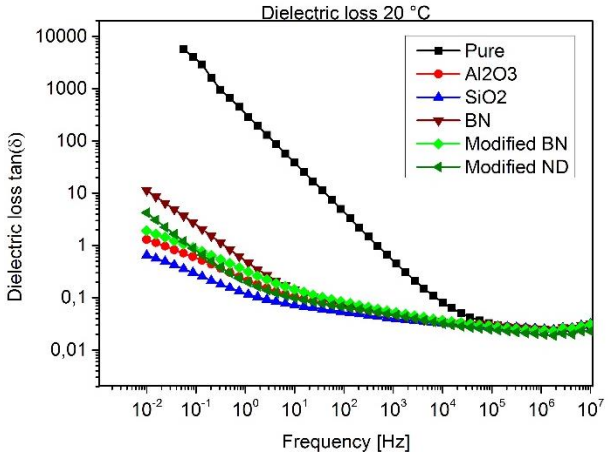

Figure 40: Dielectric loss of the nanocomposites at 20 °C.

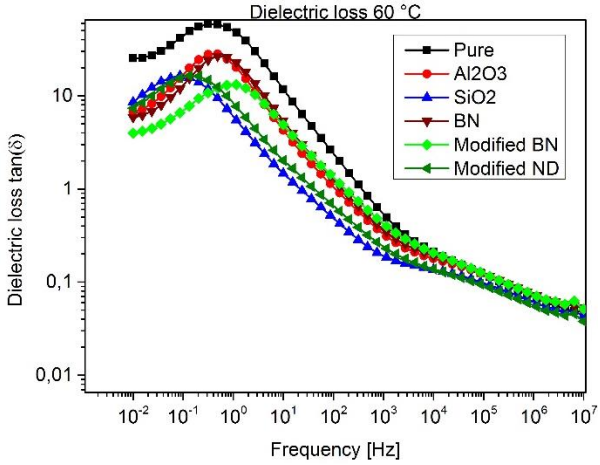

Figure 41: Dielectric loss of the nanocomposites at 60 °C

Table 4: Dielectric loss tan (δ) of the nanocomposites at −20, 20 and 60 °C, and 50 Hz.

Specimen ↓ / T →	**-20 °C**	**20 °C**	**60 °C**
Copolymer	9.5	8.43	3.86
10 wt.-% Al_2O_3	0.011	0.07	1.54
10 wt.-% SiO_2	0.012	0.06	0.67
10 wt.-% BN	0.02	0.08	1.88
10 wt.-% mod. BN	0.11	0.09	1.9
10 wt.-% mod. ND	0.03	0.07	0.92

Figures of all results concerning the real part of the permittivity, the imaginary part of the permittivity and the dielectric of the nanocomposites (detailed for the individual specimens) have been summarized in the appendix.

4.8 Contact angle measurements

4.8.1 Measurement Principle

A common way to determine the free surface energy is from drop-shape analyses / contact angles measurements of test liquids on a substrate (Figure 42). Two different methods exist: In one method, the droplet is dropped from a needle onto the surface. In the other method, the substrate is brought in direct contact with the needle tip, from which the droplet is picked up.[81] Typical liquids for contact angles measurement are diiodomethane as nonpolar liquid, and deionized water as well as ethylene glycol as polar liquids. From the contact angles of the liquids on the sample, the free surface energy can calculated, including the polar and nonpolar parts on the surface. [82]

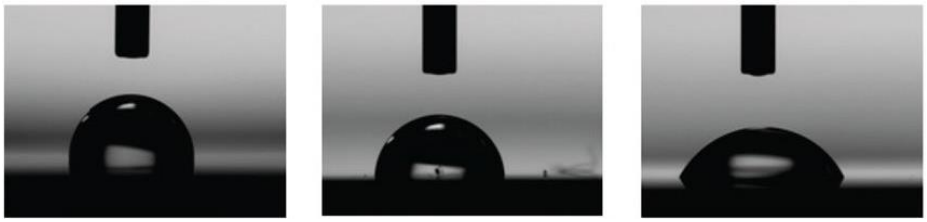

Figure 42: Contact angle measurements with the test liquid water on different substrates, comprising hydrophobic surfaces (left) and hydrophilic surfaces (right).[83]

4.8.2 Measurement Set-up

For the measurements, diiodomethane and water were used. The surface energy was calculated according to Owens-Wendt.[84] The surface

energy of the copolymer was pronouncedly low and exhibited the lowest value of the series of 12.34±1.72 $mN \cdot m^{-1}$ (Figure 42; Table 5). This observation has been referred to the orientation of the hydrophobic side-chains towards the surface (chapter 3.6). By the addition of nanoparticles, the surface energy was increased to approx. 20 $mN \cdot m^{-1}$ for all nanocomposites, which still may be considered a value for hydrophobic surfaces (pure NonOx polymer: 22 $mN \cdot m^{-1}$; PTFE: 24 $mN \cdot m^{-1}$; polypropylene: 30 $mN \cdot m^{-1}$).[57] Notably, the nanocomposites showed lower polar fractions of the surface energy than the unfilled copolymer.

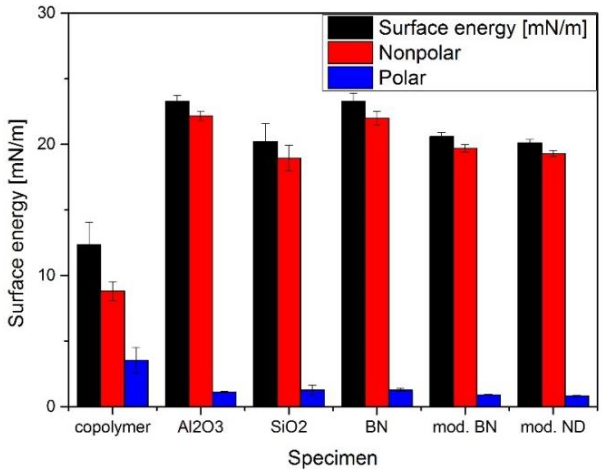

Figure 43: Surface energies of the nanocomposites.

Table 5: Surface energy of the nanocomposites, with nonpolar and polar fractions.

Specimen ↓ / Surface Energy →	**Surface energy [$mN \cdot m^{-1}$]**	**Nonpolar part of the surface energy [$mN \cdot m^{-1}$]**	**Polar part of the surface energy [$mN \cdot m^{-1}$]**
Copolymer	12.34 ± 1.72	8.81 ± 0.72	3.54 ± 1
10 wt.-% Al_2O_3	23.28 ± 0.44	22.17 ± 0.37	1.11 ± 0.06
10 wt.-% SiO_2	20.21 ± 1.36	18.95 ± 0.98	1.26 ± 0.37
10 wt.-% BN	23.27 ± 0.61	22.0 ± 0.5	1.27 ± 0.11
10 wt.-% mod. BN	20.59 ± 0.32	19.69 ± 0.28	0.9 ± 0.04
10 wt.-% mod. ND	20.11 ± 0.26	19.28 ± 0.22	0.83 ± 0.04

4.9 Thermal Conductivity

4.9.1 Theoretical Aspects

Thermal energy in polymers is transported via elastic waves in the solid state and via the energy transfer by the collision between molecules. The thermal conductivity λ quantifies the transport of energy in a material (Derye equation; equation 11, with c_p as thermal capacity, ρ as density, c as speed of sound, and l as distance between molecules).

$$\lambda = c_p \cdot \rho \cdot c \cdot l \qquad (11)$$

The unit for the thermal conductivity is $W \cdot m^{-1} \cdot K^{-1}$ or $J \cdot cm^{-1} \cdot s^{-1} \cdot K^{-1}$. For measurements of thermal conductivity, the specimen needs to be placed between a cooling and a heating plate, such that there is a defined temperature gradient present between the two plates. Through thermal elements, the temperature difference between the two plates is measured. For better contact between plates and specimen, pressure is applied.[85]

In a recent study, the thermal conductivity of epoxy resins containing Al_2O_3 nanoparticles (5 and 40 wt.-%) was investigated. For the unfilled epoxy resin, a thermal conductivity of 0.2 $W \cdot m^{-1} \cdot K^{-1}$ was found, while the values increased in the nanocomposites to 0.31 (5 wt.-% of Al_2O_3) and 0.45 $W \cdot m^{-1} \cdot K^{-1}$ (40 wt.-% of Al_2O_3). [86]

4.9.2 Thermal Conductivity of the Nanocomposites

The thermal conductivity of pNonOx$_{75}$-*stat*-pDc$^{=}$Ox$_{25}$ and the pNonOx$_{75}$-*stat*-pDc$^{=}$Ox$_{25}$ nanocomposites were measured in duplicate for each specimen at 30, 60, and 90 °C (Figures 44 to 46; Table 6).

The unfilled nanocomposite had a thermal conductivity of approx. 0.15 $W \cdot m^{-1} \cdot K^{-1}$, which is in the same range like epoxy resins. In particular the addition of BN and modified BN had a significant positive effect to the

thermal conductivity of copoly(2-oxazoline); the corresponding nanocomposites exhibited a thermal conductivity of approx. 0.20 $W \cdot m^{-1} \cdot K^{-1}$, highlighting the exceptionally high thermal conductivity of this material.

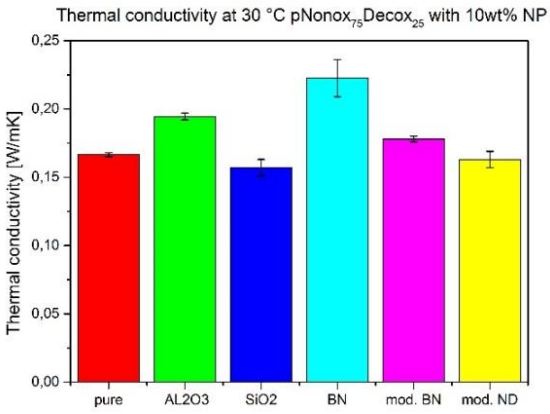

Figure 44: Thermal conductivity of the nanocomposites at 30 °C.

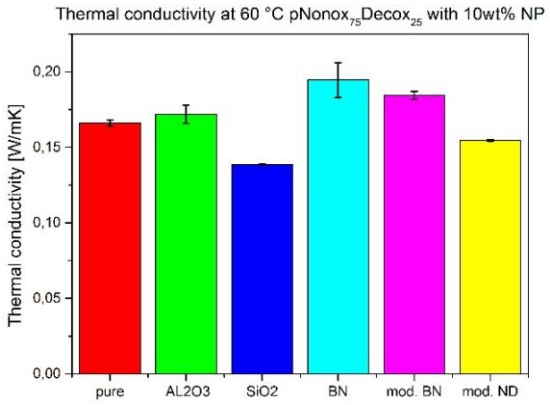

Figure 45: Thermal conductivity of the nanocomposites at 60 °C.

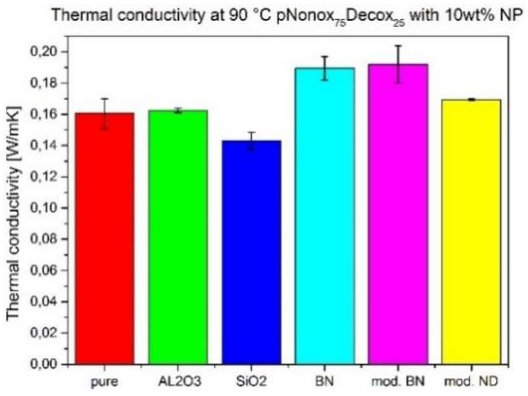

Figure 46: Thermal conductivity of the nanocomposites at 90 °C.

Table 6: Thermal conductivity at 30, 60 and 90 °C of the nanocomposites

Specimen ↓ / T →	30 °C	60 °C	90 °C	Ø h [mm]
Copolymer	0.167	0.166	0.161	1.72
10 wt.-% Al_2O_3	0.195	0.172	0.163	1.62
10 wt.-% SiO_2	0.157	0.139	0.143	1.65
10 wt.-% BN	0.223	0.195	0.190	1.66
10 wt.-% mod. BN	0.178	0.185	0.192	1.99
10 wt.-% mod. ND	0.163	0.155	0.170	1.96

4.10 Moisture adsorption

For the moisture adsorption study the nanocomposites will be placed in an oven with 50 °C and 50% humidity. The specimens were weighed before placement in the oven, and that the moisture adsorption was checked gravimetrically until weight constant was achieved (Equation 12).[87]

$$M_t(\%) = \frac{m_t - m_0}{m_0} \cdot 100 \qquad (12)$$

Three different adsorption ranges could be observed upon storing the specimens under the conditions specified hereinabove (Figure 47). The highest water uptake occurred in the nanocomposite with un-modified SiO_2, in which a water uptake of 0.8 wt.-% after 24 h and an equilibrium water content of 0.5 wt.-% were observed. The second range includes the unfilled copolymer and the nanocomposites with both types of hBN and alumina. These specimens only had a low water uptake of around 0.4 wt.-% in the beginning and an equilibrium water uptake of approx. 0.2 wt.-%. The nanocomposite with modified nanodiamonds had a significant decrease of 0.6 wt.-% of the initial weight over the study. This weight loss must be referred to the formation of volatile compounds and is assumed to be indicative of the instability of the nanodiamond filler under the conditions applied.

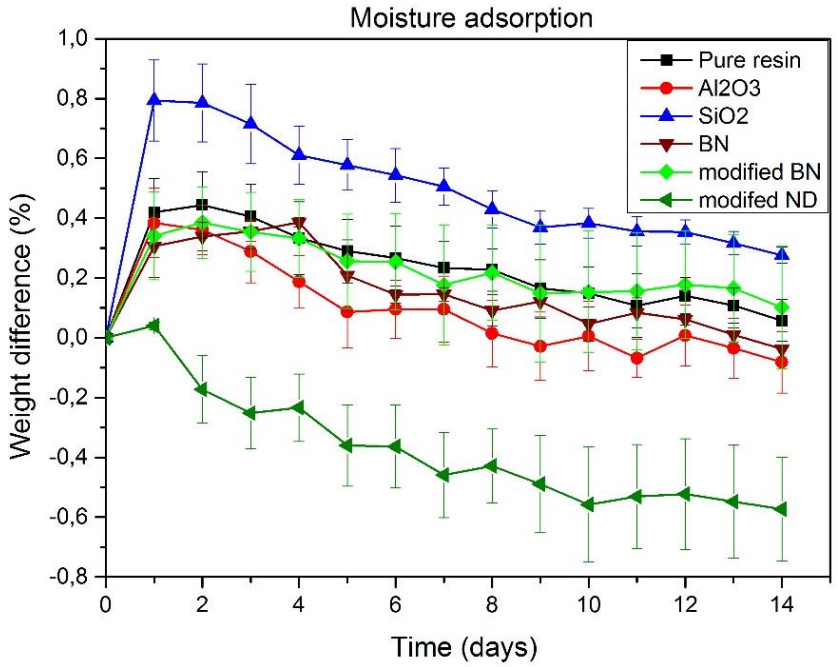

Figure 47: Weight difference of the nanocomposites upon storage at 50 °C and 50% humidity over 14 days.

Table 7: Weight difference of the nanocomposites upon storage at 50 °C and 50 % humidity (comparison of day 1 and day 14).

Specimen	Difference in % after day 1	Difference in % after day 14
Copolymer	+0.42	+0.058
10 wt.-% Al_2O_3	+0.384	–0.082
10 wt.-% SiO_2	+0.794	+0.276
10 wt.-% BN	+0.1	+0.0
10 wt.-% mod. BN	+0.341	+0.101
10 wt.-% mod. ND	+0.04	–0.573

5. Conclusions and Outlook

The scope of this master thesis was to investigate poly(2-oxazoline)s for a possible application as a ‘green’ and environmentally friendly alternative to epoxy resins in the application field of high-voltage insulation materials. In order to improve the insulation properties and the thermal conductivity of the corresponding nanocomposites, 5 different types of nanoparticles were added to the copoly(2-oxazoline)s, namely (native) silica, (native) alumina, (native and modified) boron nitride, and (modified) nanodiamonds.

The targeted copoly(2-oxazoline) should have a low surface energy and side-chain olefin functionalities. The monomers 2-nonyl-2-oxazoline NonOx and 2-dec-9’-enyl-2-oxazoline Dc$^{=}$Ox were synthesized according to the Henkel patent from the solvent-free reaction of decanoic acid/10-undecenoic acid with ethanolamine, with Ti(IV)butoxide as catalyst. Both fatty acids were obtained from renewable resources. Via the microwave-assisted, pseudo-living cationic ring-opening polymerisation of NonOx and Dc$^{=}$Ox, the copolymer of the targeted composition pNonOx$_{75}$-*stat*-pDc$^{=}$Ox$_{25}$ was synthesized. For the production of crosslinked nanocomposites, the polymer pNonOx$_{75}$-*stat*-pDc$^{=}$Ox$_{25}$ was fine-crushed in a mortar, followed by the addition of the crosslinker, the nanoparticles, and the photoinitiator. The reaction mixture was mixed vigorously. This mixture was transferred into a steel template, which was put into a panel press at 180 °C and 35 bar pressure for 15 min for the breakdown-voltage and permittivity specimen and 30 min for the thermal conductivity specimen, respectively. The specimens were taken out of the template and illuminated.

For the characterization of the manufactured specimens as insulator material, several measurements were performed. These investigations comprised DSC measurements, which showed that the added nanoparticles did not affect the thermic response of the polymer (matrix).

The electrical breakdown strength is an indicator for the long-term life of a dielectric. The AC breakdown strength for all nanocomposites was in the range of 45 kV·mm^{-1}. Notably, commercially available epoxy resins such

as CY 1300 exhibit an AC breakdown strength in the same range (60 $kV \cdot mm^{-1}$). In contrast to the uniformity of AC breakdown strength, the DC breakdown strength of the copoly(2-oxazoline)-based nanocomposites was found to vary on the type of nanoparticles (Figure 48). The highest DC breakdown strength, namely approx. 100 $kV \cdot mm^{-1}$, was achieved by the addition of 10 wt-% of SiO_2, whereas the unfilled copoly(2-oxazoline) reached only 60 $kV \cdot mm^{-1}$. Pure epoxy resins such as CY231 have a DC breakdown strength in the range of 150 $kV \cdot mm^{-1}$.

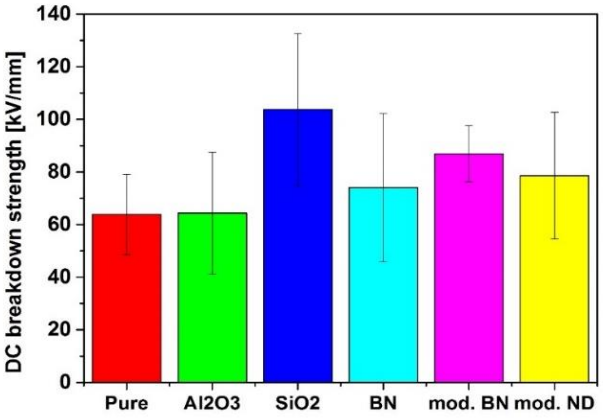

Figure 48: DC breakdown strength of the copolymer and the nanocomposites.

The permittivity was measured over a broad frequency range at –20, 20, and
60 °C. The real part of the relative permittivity increased with decreasing frequencies lower than 100 Hz at 20 and 60 °C. The increase of the permittivity at low frequencies is associated with irregularities in the material like grain boundaries and interfacial polarization, which is highly sensitive to water impurities. At the industrial standard of 50 Hz and 20 °C, the unfilled copolymer as well as all nanocomposites showed a permittivity in the same range like epoxy resins and polyamides.

The imaginary part of the relative permittivity was found to be similar to the real part of the permittivity: It increases with decreasing frequencies and increasing temperature. Notably, the nanocomposites containing SiO_2, Al_2O_3, and modified BN exhibited the lowest imaginary parts of the permittivity. At the other side of the spectrum, the unfilled copolymer

exhibited the highest values of the imaginary part of the permittivity at –20 and +20 °C (Figure 49). At the highest measured temperature of 60 °C, the unfilled copolymer and the nanocomposites exhibited very comparable behaviour.

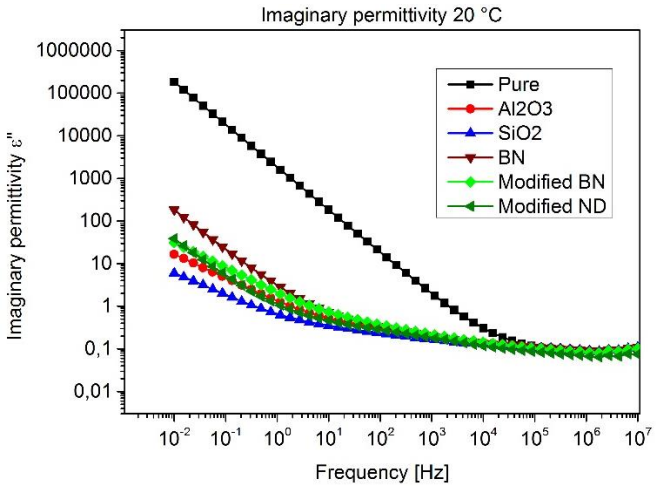

Figure 49: Imaginary part (permittivity) of the nanocomposites at 20 °C.

The dissipation factor tan (δ), which quantifies the relation of the imaginary and the real part of the permittivity, illustrates the loss of insulation properties for values tan (δ) >> 1. Such values can be observed for the unfilled copolymer already at temperatures of –20 and +20 °C at frequencies lower than 10^4 Hz. Overall, the dielectric loss factor for all nanocomposites as well as for the unfilled copolymer increases with lower frequencies and higher temperature. The nanocomposites can be considered as insulators at frequencies above 1 Hz at temperatures of –20 and +20 °C, and at frequencies higher 100 Hz at 60 °C. Hence, there is a significant impact of the added nanoparticles on the insulation properties of the copoly(2-oxazoline)s (Table 4).

Measurements of the surface energy of the copolymer and the nanocomposites revealed that, due to the preferred orientation of the hydrophobic side-chains towards the surface (*hydrophobic recovery*), the unfilled copolymer has the lowest value, while the addition of nanoparticles increased the surface energy due to interactions of the nanoparticles and the polymer matrix.

Table 8: Dielectric loss tan (δ) of the nanocomposites at 50 Hz and −20, 20 and 60 °C.

Specimen ↓ / T →	**-20 °C**	**20 °C**	**60 °C**
Copolymer	9.5	8.43	3.86
10 wt.-% Al_2O_3	0.011	0.07	1.54
10 wt.-% SiO_2	0.012	0.06	0.67
10 wt.-% BN	0.02	0.08	1.88
10 wt.-% mod. BN	0.11	0.09	1.9
10 wt.-% mod. ND	0.03	0.07	0.92

The thermal conductivity of the copolymer and nanocomposites is of high relevance for the application as insulators in high-temperature applications. The unfilled copoly(2-oxazoline) has a thermal conductivity of 0.15 $W \cdot m^{-1} \cdot K^{-1}$, which is in the same range like epoxy resins. Nanocomposites containing BN nanoparticles (native or modified) show an increased thermal conductivity of approx. 0.2 $W \cdot m^{-1} \cdot K^{-1}$.

The water uptake of the copolymer and the nanocomposites was measured in a humidity chamber at 50 °C and 50% humidity. After 24 h, the silica-filled nanocomposite had the highest water uptake of 0.8 wt.-%, which decreased over the next 13 days to 0.4 wt.-%. The unfilled copolymer as well as the nanocomposites with hBN and alumina formed a second group of adsorption class. Their water uptake was approx. 0.4 wt.-% after 24 h, and the average water uptake over 14 days was approx. 0.2 wt.-%. The nanocomposite with modified nanodiamonds lost approx. 0.6 wt.-% over the course of the study. The weight loss can be assumed to originate from the instability of the nanodiamond filler under the conditions.

Overall, the addition of nanoparticles such as boron nitride to a moderately crosslinked copoly(2-oxazoline) improves the DC breakdown stability, the thermal conductivity, as well as the insulation properties (quantified by the dielectric loss factor) and lowers the water uptake. Further potential strategies to improve the properties of the nanocomposites comprise the manufacturing process, aiming to, e.g., accomplish a more homogenous distribution of the nanoparticles through extrusion or analogous processes.

6. Kurzfassung

Das Ziel der vorliegenden Arbeit war der Vergleich poly(2-oxazolin)-basierender Harze mit Epoxidharzen in Hinblick auf potentielle Anwendungen im Hochspannungssektor als Isolationsmaterial. Die Motivation für die Suche nach Alternativen begründet sich auf die negativen gesundheitlichen Auswirkungen des Bisphenol A, welches als Diglycidylether in Epoxidharzen enthalten ist. Poly(2-oxazolin)e können als gesundheitlich unbedenklich eingestuft werden.

Die Ausgangsstoffe für die Monomere 2-Nonyl-2-oxazolin und 2-Dec-9‘-enyl-2-oxazolin können aus erneuerbaren Rohstoffen gewonnen werden. Deren Copolymerisation kann in rezyklierbaren ionischen Flüssigkeiten erfolgen, sodass eine ‚grüne Synthese‘ der Copoly(2-oxazolin)e möglich ist. Diese Copolymere haben eine geringe Oberflächenenergie, sodass die Einlagerung von Wasser minimiert wird. Mittels der UV-induzierten Thiol-en Reaktion zwischen dem Copolymer und einem bisfunktionalem Thiol konnten dreidimensionale Netzwerke dargestellt werden. Um die Isolationseigenschaften zu erhöhen, wurden dem Poly(2-oxazolin) verschiedene Nanopartikel zugesetzt. Bei den Nanopartikeln handelte es sich um kommerzielles Silika, Alumina und Bornitrid sowie modifiziertes Bornitrid und Nanodiamanten.

Die thermische Leitfähigkeit und die Durchschlagsspannung (AC bzw. DC) der poly(2-oxazolin)-basierenden Harze und Nanokomposite waren mit denen von Epoxidharzen vergleichbar. Die Resultate der Permittivitätsmessungen zeigten, dass das reine Copoly(2-oxazolin) nur bei niedrigen Temperaturen und hohen Frequenzen als Isolator fungiert. Im Gegensatz dazu zeigten die Nanokomposite unter industriellen Standardbedingungen gute Isolationseigenschaften. Die Wasseraufnahmestudie ergab, dass nur sehr geringe Mengen an Wasser von den Nanokompositen und dem Copolymer aufgenommen wurden. Unter Berücksichtigung aller Ergebnisse lässt sich zusammenfassend erkennen, dass Nanokomposite mit Bornitrid die beste Kombination von Eigenschaften für deren Einsatz als Isolatoren in der Hochspannungstechnologie aufweisen.

7. Abstract

The aim of this thesis was the comparison of poly(2-oxazoline)-based resins with epoxy resins with special regard to potential applications in the high-voltage sector as an insulating material. The motivation for the search for alternatives to epoxy resins is based on the negative health effects of bisphenol A, which is contained as diglycidyl ether in epoxy resins. Poly(2-oxazoline)s can be classified as harmless to health.

The starting materials for the monomers 2-nonyl-2-oxazoline and 2-dec-9'-enyl-2-oxazoline can be obtained from renewable raw materials. Their copolymerization can be carried out in recyclable ionic liquids, such that a 'green synthesis' of the copoly(2-oxazoline)s is possible. These copolymers have a low surface energy, aiming at minimized amounts of water uptake. By means of the UV-induced thiol reaction between the copolymer and a bisfunctional thiol, three-dimensional networks could be produced. In order to increase the insulation properties, various nanoparticles were added to the poly(2-oxazoline)s. The nanoparticles were commercial silica, alumina and boron nitride as well as modified boron nitride and nanodiamonds.

The thermal conductivity and the breakdown voltage (AC or DC) of the poly(2-oxazoline)-based resins and nanocomposites were comparable with those of epoxy resins. The results of the permittivity measurements showed that the pure copoly(2-oxazoline) acts as an insulator only at low temperatures and high frequencies. In contrast, the nanocomposites showed good insulation properties under industrial standard conditions. The water absorption study showed that only very small amounts of water were absorbed by the nanocomposites and the copolymer. Taking into account all the results, it can be seen that nanocomposites with boron nitride have the best combination of properties for their use as insulators in high-voltage technology.

8. Experimental Part

8.1 Used Materials

The suppliers of the chemicals have been summarized in Table 8.

Table 9: Used chemicals.

Chemicals	Supplier	Purity	Side note
10-Undecenoic acid	Sigma-Aldrich, Austria	97%	
2-Aminoethanol	Sigma-Aldrich, Austria	98%	
Acetonitrile	Carl Roth, Austria	99.50%	
Chloroform	AnalaR Normapur	99.20%	
Decanoic acid	SFC	98%	
Dichloromethane	Fischer Chemicals	>99%	
Glycoldimercaptoacetate	Bruno Bock, Deutschland	90%	
Methanol	Chem Lab	HPLC	
Methyl tosylate	Sigma-Aldrich, Austria	98%	distilled
Titanium(IV)butoxide	Sigma-Aldrich, Austria	99%	
Ethanol	AnalaR Normapur	96.90%	
Ethyl lactate	AnalaR Normapur	99.90%	
3SH	Abcr, Germany	95.30%	
4SH	Abcr, Germany	85%	
BN	MKnano, Canada	99.90%	
Modified BN	Nanodiamond, Israel	99.90%	
Modified ND	Nanodiamond, Israel	99.90%	
Al_2O_3	Sigma-Aldrich, Austria	99.80%	
SiO_2	Sigma-Aldrich, Austria	99.80%	

8.2 Analytical Methods

NMR analysis: The NMR spectra were recorded with a Bruker Advance III 300 MHz spectrometer in deuterated chloroform, unless specified otherwise. All spectra were calculated to the intern reference of chloroform (7.26 ppm for ^{1}H-NMR spectra and 77 ppm for the ^{13}C-NMR spectra).

IR spectroscopy: The IR measurements were recorded on a Bruker Alpha Fourier-Transform Infrared Spectrometer with ATR-module. The spectra

range was from 375 to 4000 cm^{-1} with 32 scans. The background was subtracted from the spectra.

Gel permeation chromatography: A Merck Hitachi L-6000A pump, a column from Polymer Standards Service, 8/300mm STV linear XL 5µm-grad size, and a differential refractometer Waters 410 detector were used for the GPC measurements. For calibration, a polystyrene standard from Polymer Standard Service was used. The eluent was a mixture of $CHCl_3$/Et_3N/^{iso}PrOH (94/4/2).

Electrical breakdown and permittivity measurements: The electrical breakdown and permittivity were accomplished with a OPG-100A insulating oil tester according to the IEC60156 standard. The different parameters for each measurement can be found in a more detailed fashion in the results chapter.

Humidity chamber: The water uptake study was executed in a Memmert HCP 108, at a temperature of 50 °C and a humidity of 50 % over the course of 14 d.

Panel press: For the specimen manufacturing, a Collin p 200 PV panel press was applied. The specific parameters for each specimen can be found in the experiment chapter.

SEM-EDX: The secondary electron pictures were made with a VEGA 3 TESCAN.

Microwave-assisted polymerizations: A Biotage Initiator 8 microwave reactor was used for the polymerization of the poly(2-oxazoline)s.

UV-induced crosslinking and illumination: An EFOS Novacure UV Hg/Xe lamp from EXFO was used. The lamp was placed in a distance of 10 cm between lamp and specimen, and the illumination time was adjusted for thickness of the nanocomposite with a power of 5000 $mW \cdot cm^{-2}$.

Thermal analysis: A Perkin Elmer DSC 4000 with auto sampler was used for the thermal analysis. The thermogram was recorded under nitrogen atmosphere at a temperature range between 30 and 200 °C with a heating rate of 10 $K \cdot min^{-1}$. Only the first scan was used for the calculations.

8.3 Synthesis of the monomers

8.3.1 Synthesis of 2-Nonyl-2-oxazoline

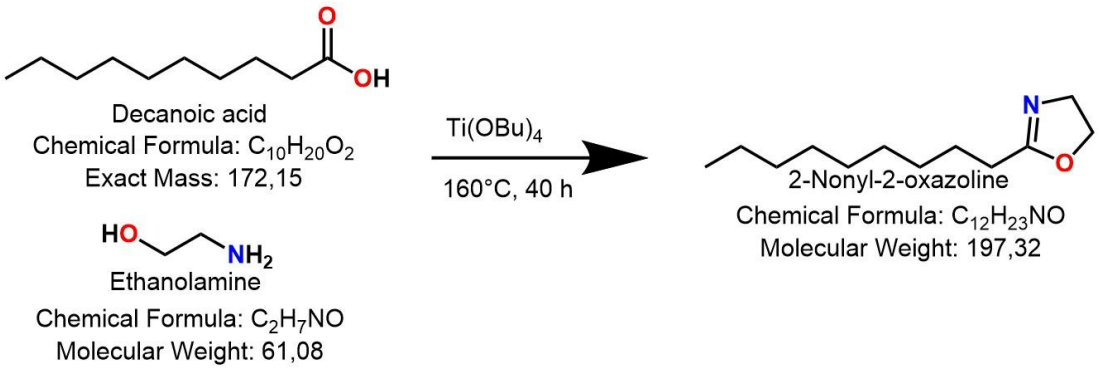

Figure 50: Synthesis of 2-nonyl-2-oxazoline.

The synthesis of 2-nonyl-2-oxazoline followed the protocol described in the Henkel patent.[39] Decanoic acid (100 g; 0.58 mol) was melted at 40 °C and transferred into a 500 mL flask. Afterwards, ethanolamine (53.1 g; 0.87 mol) and titanium(IV)-*n*-butoxide (2.00 g; 5.8 mmol) was added. The reaction mixture was heated up to 160 °C under reflux and stirred overnight. After 16 and 20 h, respectively, further amounts of titanium(IV)-*n*-butoxide (2.00 g; 5.8 mmol) were added. After 24 h stirring under reflux conditions, the cooler was removed, and the reaction mixture was stirred at 160 °C for 20 h. Purification of the reaction mixture and recovery of the product was achieved by distillation under reduced pressure (< 2 mbar) at a temperature of 175 °C.

^{1}H NMR (300 MHz, $CDCl_3$): δ (ppm) = 0.87 (3 H, t, -C*H*$_3$), 1.25 (12 H, s, -C*H*$_2$-), 1.58–1.66 (2 H, m, -C*H*$_2$-CH$_3$), 2.25 (2 H, t, -C(=)-C*H*$_2$-CH$_2$-), 3.81 (2 H, t, -O-CH$_2$-C*H*$_2$-N=), 4.21 (2 H, t, -O-C*H*$_2$-CH$_2$-N=).

^{13}C NMR (75 MHz, $CDCl_3$): δ (ppm) = 14.1, 20.4, 22.7, 29.3, 29.6, 31.9, 32.4, 53.8, 68.1, 173.7.

IR (ATR): ν (cm^{-1}) = 2924, 2849, 1463, 1240, 1082.

8.3.2 Synthesis of 2-(Dec-9´-enyl)-2-oxazoline

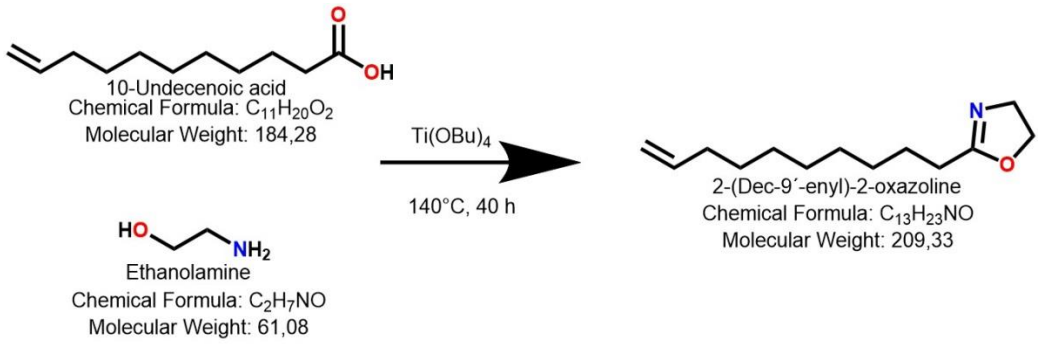

Figure 51: Synthesis of 2-(dec-9´-enyl)-2-oxazoline.

According to the Henkel patent,[39] 10-undecenoic acid (100 mL; 91.2 g; 0.5 mol) was transferred into a 500 mL flask, ethanolamine (45.3 g; 44.8 mL; 0.74 mol) and titanium(IV)-n-butoxide (0.84 g; 2.5 mmol) were added. The reaction mixture was heated to 140 °C under reflux conditions and stirred for 20 h. After 16 and 20 h, titanium(IV)-n-butoxide (2.00 g; 5.8 mmol) was added. Subsequently, the cooler was removed and the reaction mixture was stirred at 140 °C for 20 h. Purification of the reaction mixture and recovery of the product was achieved by distillation under reduced pressure (< 2 mbar).

^{1}H-NMR (300 MHz, $CDCl_3$): δ (ppm) = 1.20-1.40 (10 H, m, -CH_2-), 1.52-1.68 (2 H, m, -CH_2-C*H*$_2$-CH_2-C (=)-), 1.96-2.02 (2 H, m, -CH_2-C*H*$_2$-CH=), 2.24 (2 H, t, -C(=)-C*H*$_2$-CH_2-), 3.79 (2 H, t, -O-C*H*$_2$-CH_2-N=), 4.19 (2 H, t, -O-CH_2-C*H*$_2$-N=), 4.86-5.00 (2 H, m, -CH=C*H*$_2$), 5,90-5.70 (1 H, m, -C*H*=CH_2).

^{13}C NMR (75 MHz, $CDCl_3$): δ (ppm) = 20.4, 29.3, 29.6, 32.4, 33.9, 53.8, 68.1, 115.7, 139.1, 173.7

IR (ATR): ν (cm^{-1}) = 2921, 2852, 1641, 1463, 1430, 1182, 1160, 909, 772, 721.

8.4 Synthesis of pNonOx$_{75}$-*stat*-pDc$^{=}$Ox$_{25}$

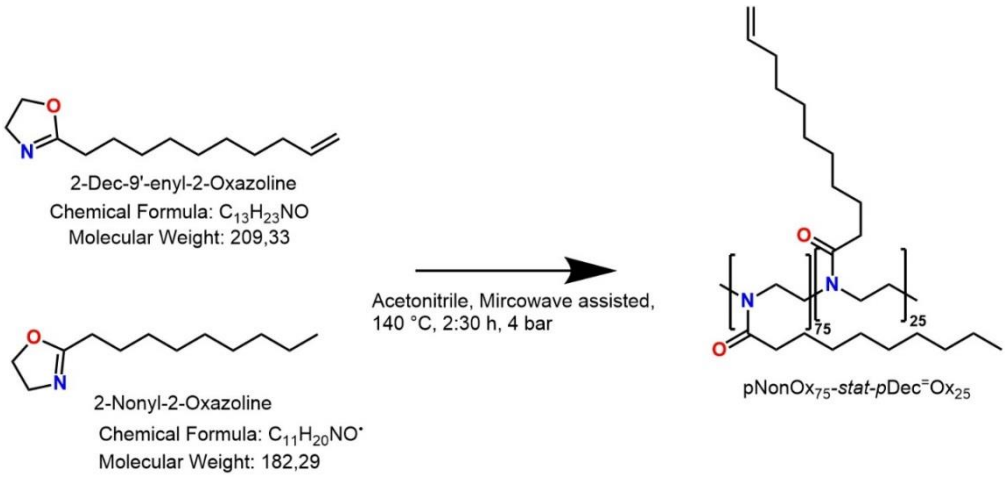

Figure 52: Microwave-assisted polymerisation of pNonOx$_{75}$-*stat*-pDc$^{=}$Ox$_{25}$.

For the synthesis of the copolymer(2-oxazoline) pNonOx$_{75}$-*stat*-pDc$^{=}$Ox$_{25}$, a 20 ml Biotage reaction vessel was placed in a drying oven for 30 min at 60 °C. 7.388 g (0.04 mol) NonOx, 2.612 g (0.0125 mol) Dc$^{=}$Ox, and 92.97 mg (5 mmol) MeTos were weighed in the reaction vessel. 10 mL of acetonitrile were added, and the vial was crimped. The closed reaction vessel was placed in the Biotage microwave reactor and heated at 140 °C for 2.5 h. Afterwards, the solvent was evaporated under high vacuum (< 2 mbar).

^{1}H-NMR (300 MHz, CDCl$_3$): δ (ppm) = 1.20-1.40 (10 H, m, -CH$_2$-), 1.52-1.68 (2 H, m, -CH$_2$-C*H$_2$*-CH$_2$-C(=)-), 1.96-2.02 (2 H, m, -CH$_2$-C*H$_2$*-CH=), 2.24 (2 H, t, -C(=)-C*H$_2$*-CH$_2$-), 3.79 (2 H, t, -O-C*H$_2$*-CH$_2$-N=), 4.19 (2 H, t, -O-CH$_2$-C*H$_2$*-N=), 4.86-5.00 (2 H, m, -CH=C*H$_2$*), 5,90-5.70 (1 H, m, -C*H*=CH$_2$).

^{13}C NMR (75 MHz, CDCl$_3$): δ (ppm) = 14.0, 24.6, 25.2, 28.9, 29.3, 29.5, 31.9, 32.8, 33.0, 33.7, 43.1, 45.2, 114.1, 139.0, 173.2, 173.8.

IR (ATR): ν (cm^{-1}) = 2921, 2852, 1641, 1463, 1430, 1182, 1160, 909, 772, 721.

GPC: M_n = 7.3 kDa; M_w = 16.4 kDa; M_w/M_n = 2.24.

8.5 Manufacturing of Test Specimens

The polymer pNonOx$_{75}$-*stat*-pDc$^{=}$Ox$_{25}$ was fine-crushed in a mortar, followed by the addition of the crosslinker, the different of types nanoparticles, and the photoinitiator. The reaction mixture was mixed vigorously. This mixture was transferred into a steel template. For the breakdown-voltage measurements, a ring-shaped template with a diameter of 50 mm and a height of 0.4 mm was used. For the permittivity measurements, a ring-shaped template with a diameter of 40 mm and a height of 0.3 mm was used. For the thermal conductivity measurements, a ring-shaped template with a diameter of 50 mm and a height of 2 mm was used.

The steel template was put into a panel press at 180 °C and 35 bar pressure for 15 min for the breakdown-voltage and permittivity specimen and 30 min for the thermal conductivity specimen, respectively. The specimens were taken out of the template and illuminated.

The crosslinking of the nanocomposites containing modified BN and modified nanodiamonds was insufficient, which was observed by the thin specimen for the break down voltage measurements, as well as in the thicker specimen for the thermal conductivity measurements. Hence, in an alternative processing route, the template was placed into the panel press and heated up to 130 °C for 10 min, cooled down to 40 °C, and the free space was refilled with additional mixture. Then the template was placed for a second time into the panel press and heated up to 200 °C for 30 min.

9. List of Figures

10. List of Tables

11. Appendix

11.1 List of abbreviations

AC	alternating current
BPA	Bisphenol A
Bu$^{=}$Ox	2-but-3´-enyl-2-oxazoline
C_p	heat capacity
C_p	specific thermal capacity
D	dielectric loss
D_0	dielectric capacity
DC	direct current
Dc$^{=}$Ox	2-dec-9´-enyl-2-oxazoline
DSC	differential scanning calormetry
E	electric field
E_d	dielectric strength
EtOx	2-ethyl-2-oxazoline
HVDC	high-voltage direct current
Hz	Hertz
kV	kilo Volt
l	distance between molecules
MeOx	methyl-2-oxazoline
MeTos	methyl tosylate
mod. BN	modified boron nitride
mod. ND	modified nanodiamonds
MVA	Mega Volt-Ampere
NMR	nuclear magnetic resonance
NonOx	2-nonyl-2-oxazoline
p	poly
P	polarisation
PCB	poly(chlorinated biphenylene)
Pe$^{=}$Ox	2-pent-4’ine-2-oxazoline
PhOx	2-phenyl-2-oxazoline
PI	photoinitiator

q	heat
SEM	scanning electron microscopy
T	temperature
T_g	glass-transition temperature
T_m	melting Temperature
UV	ultraviolet
x	magnification
ε"	imaginary part of the relative permittivity
ε´	real part of the relative permittivity
ε_0	permittivity of free space
ε_r	static/relative permittivity
λ	wavelength
ρ	density

11.2 Real Part of the Relative Permittivity of the Copolymer and the Nanocomposites

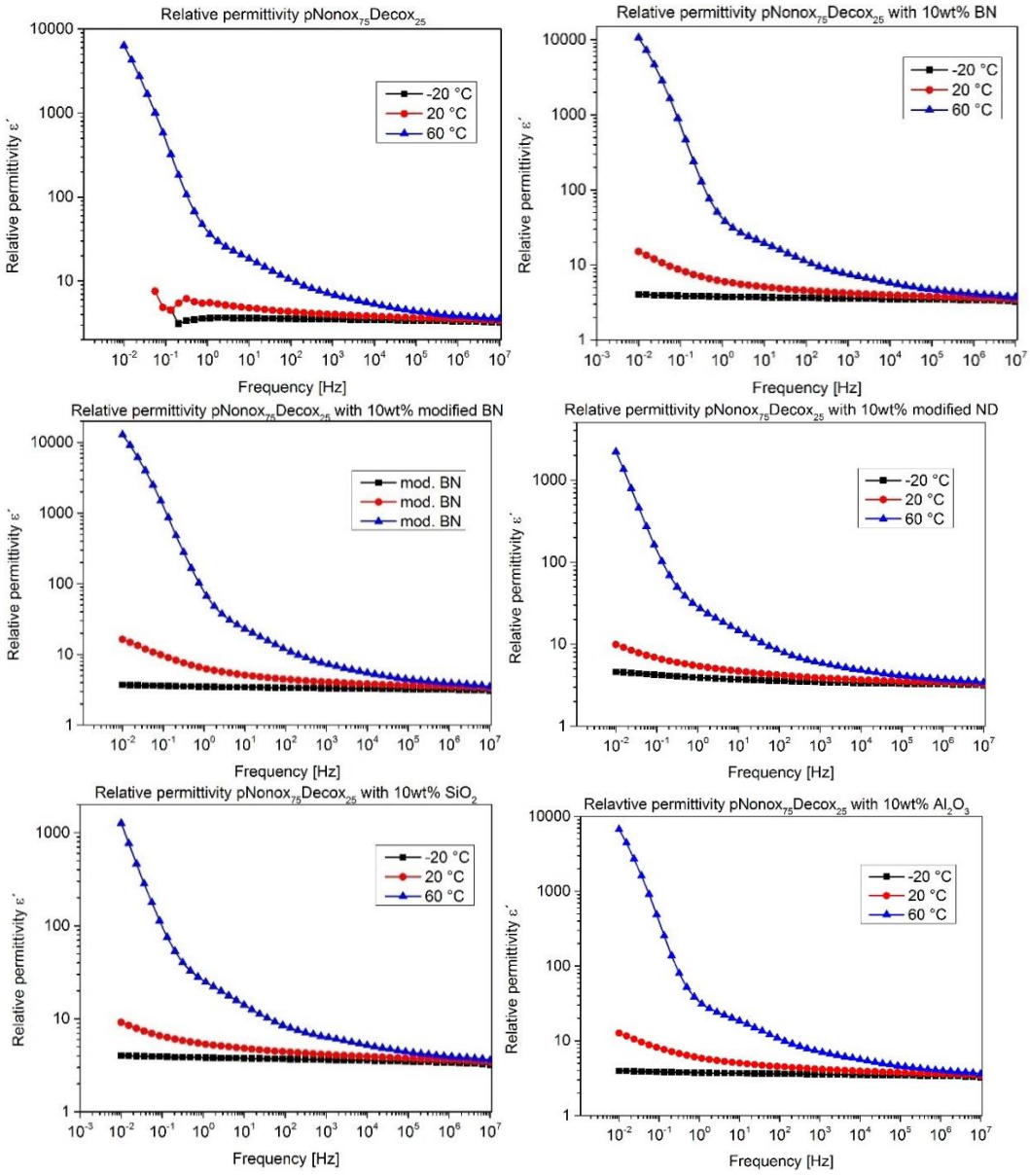

Figure 53: Real part of the relative permittivity of the copolymer and the nanocomposites.

11.3 Imaginary part of the relative permittivity from the copolymer and all nanocomposites

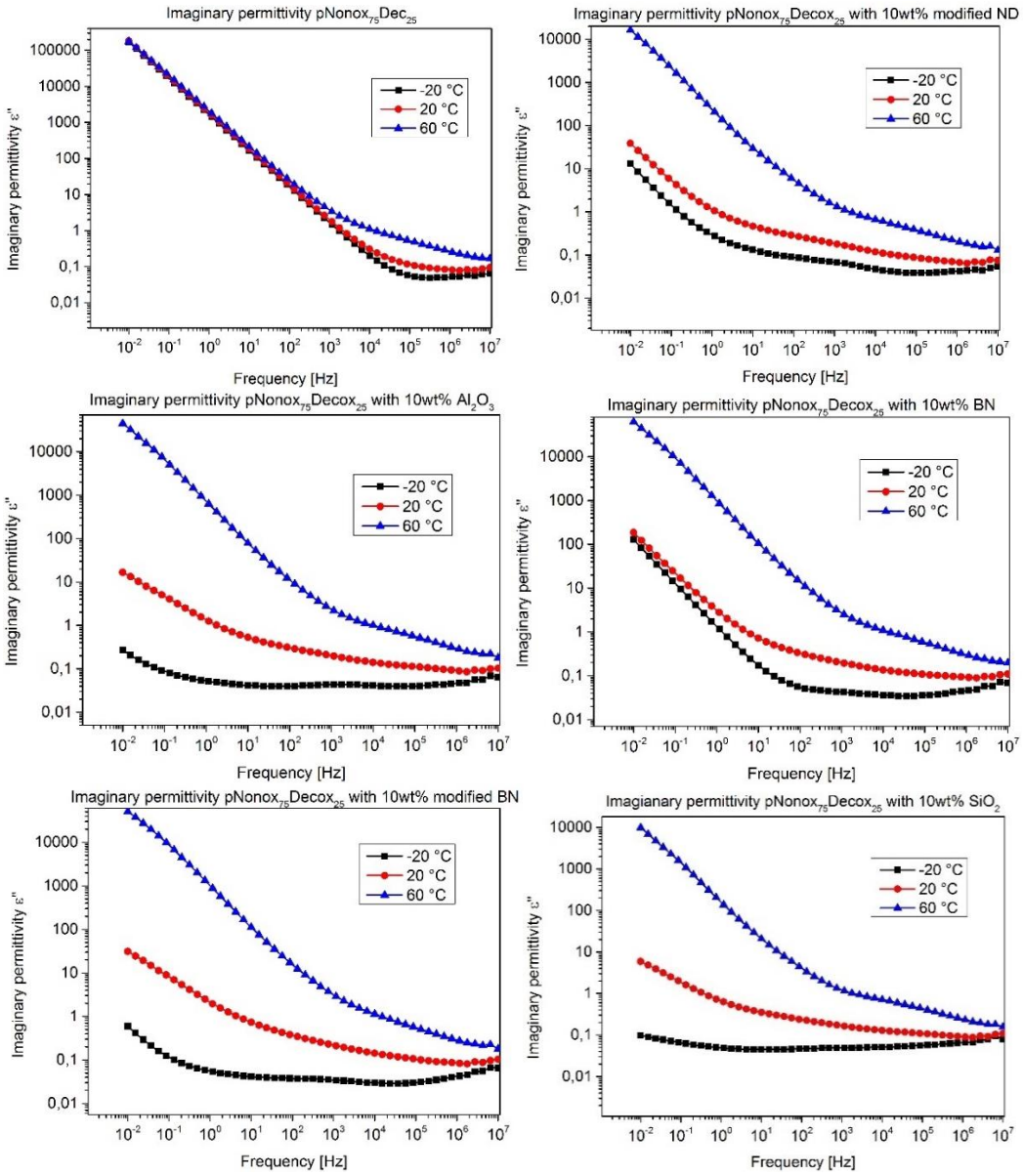

Figure 54: Imaginary part of the relative permittivity of the copolymer and the nanocomposites.

11.4 Dielectric loss of the copolymer and all nanocomposites

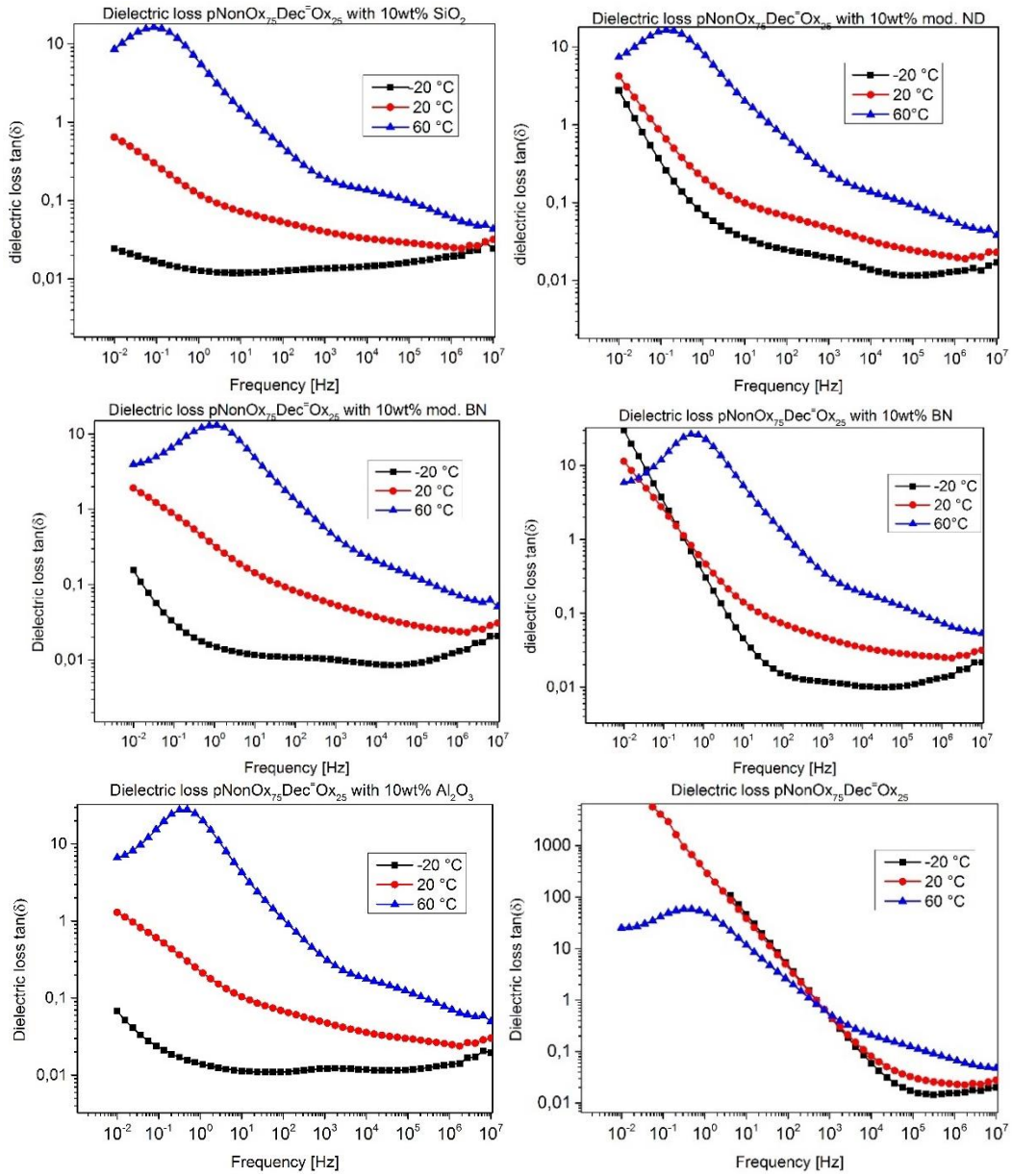

Figure 55: Dielectric loss of the copolymer and the nanocomposites.

11.5 Scanning Electron Microscopy

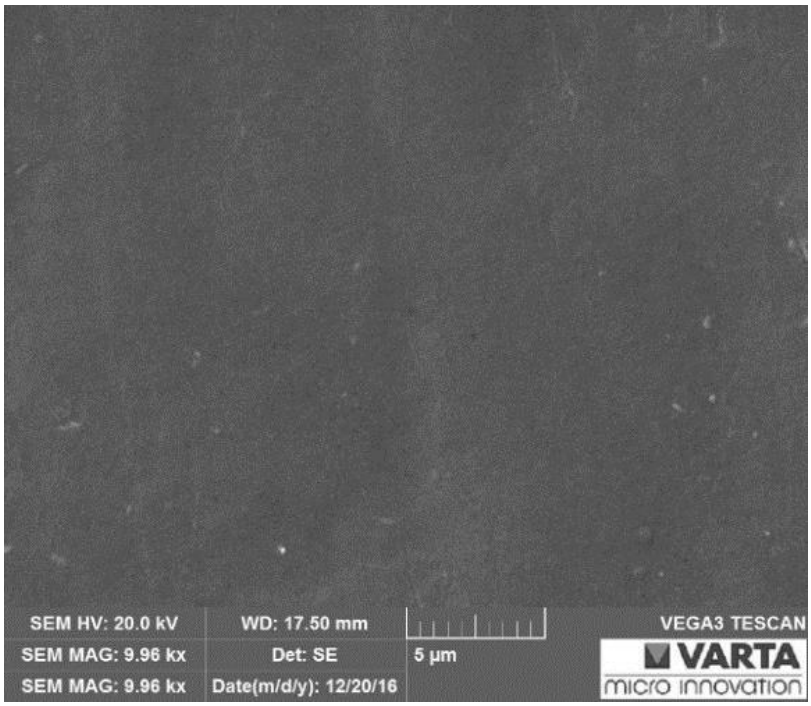

Figure 56: SEM picture of unfilled pNonOx-*stat*-pDc$^{=}$Ox.

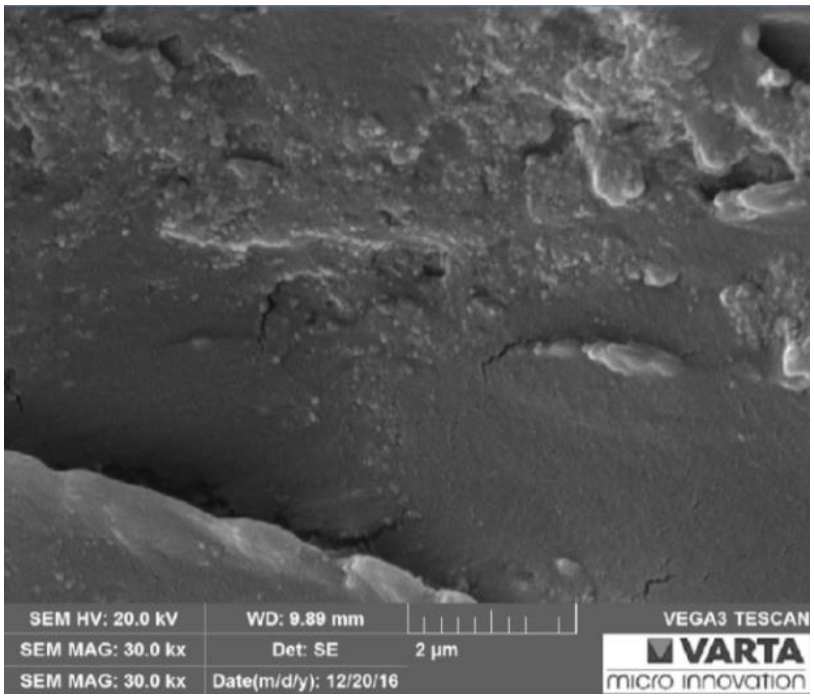

Figure 57: SEM picture of the Al_2O_3 nanocomposite.

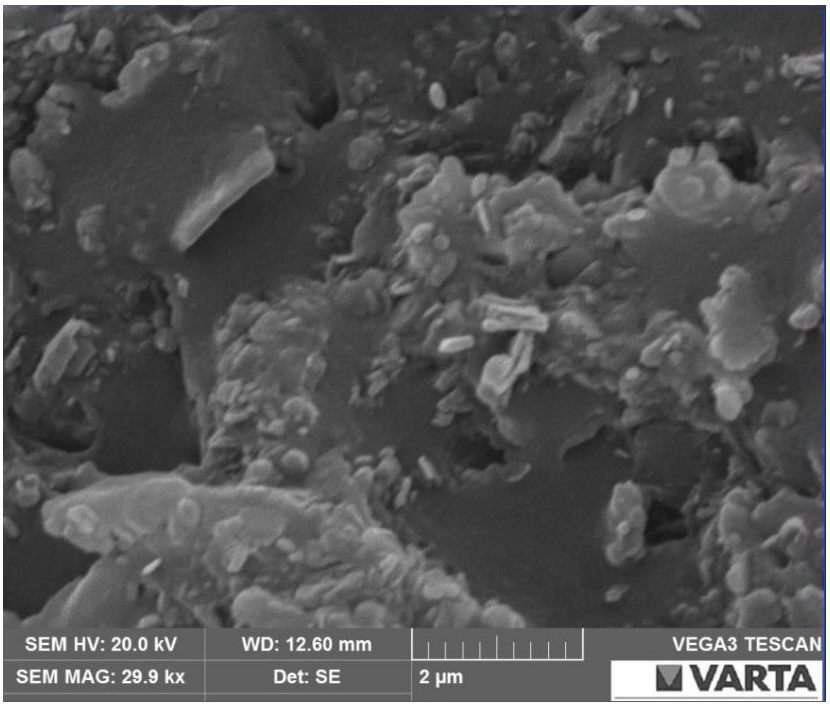

Figure 58: SEM picture of the BN nanocomposite.

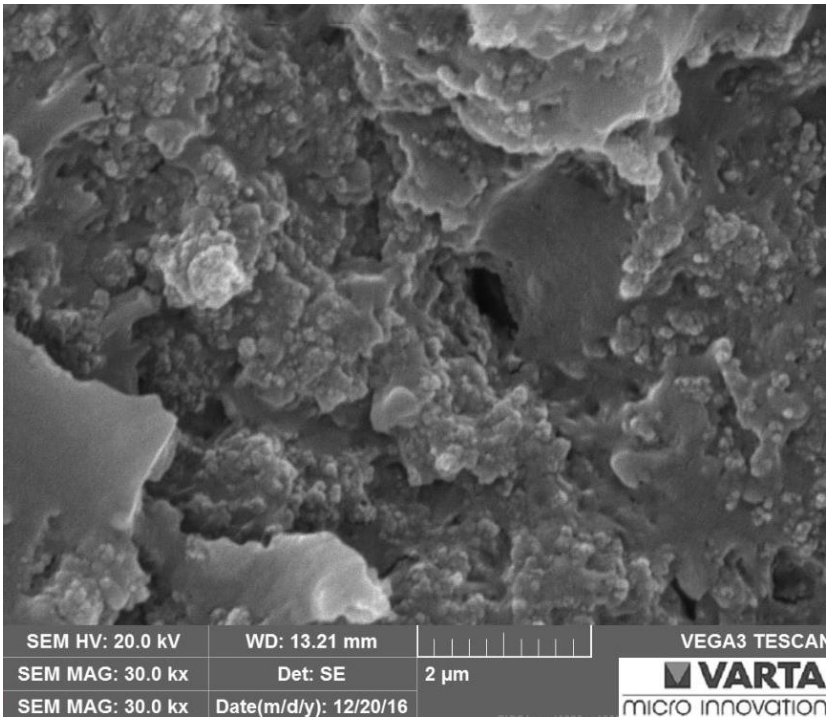

Figure 59: SEM picture of the SiO_2 nanocomposite.

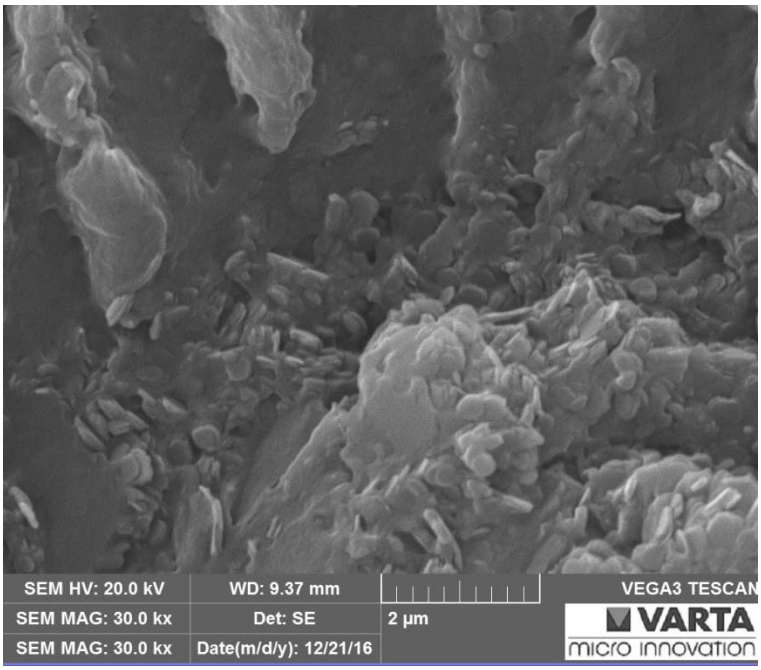

Figure 60: SEM picture of the mod. BN nanocomposite.

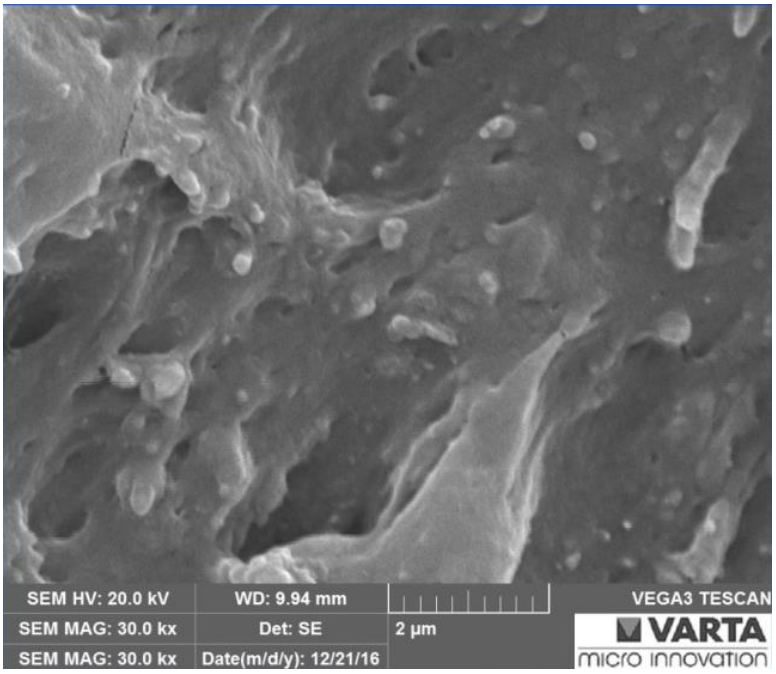

Figure 61: SEM-picture of the modified nanodiamond nanocomposite.

12. References

[1] P. Punys, R. Baublys, E. Kasiulis, A. Vaisvila, Assessment of renewable electricity generation by pumped storage power plants in EU Member States, *Renew. Sustain. Energy Rev.* **2013**, *26*, 190–200. doi:10.1016/j.rser.2013.05.072.

[2] G.C. Psarras, Hopping conductivity in polymer matrix-metal particles composites, *Compos. Part A Appl. Sci. Manuf.* **2006**, *37*, 1545–1553. doi:10.1016/j.compositesa.2005.11.004.

[3] W. Oburger, Die Isolierstoffe der Elektrotechnik, Springer-Verlag Wien, **1957**,. doi:10.1007/978-3-662-26196-5.

[4] A. Jaya, H. Berahim, T. Tumiran, R. Rochmadi, The Performance of High Voltage Insulator Based on Epoxy-Polysiloxane and Rice Husk Ash Compound in Tropical Climate Area, *Electr. Electron. Eng.* **2012**, *2*, 208–216. doi:10.5923/j.eee.20120204.06.

[5] M. Alexandre, P. Dubois, Polymer-layered silicate nanocomposites : preparation , properties and uses of a new class of materials, *Mater. Sci. Eng. A*. **2000**, *28*, 1–63.

[6] J. Dr. Sartorius, S. Hummel, A. Bracht, M. Lämmer, Nanotechnologie in Kunststoff Innovationsmotor für Kunststoffe, ihre Verarbeitung und Anwendung., *Hess. Minist. Für Wirtschaft, Verkehr Und Landesentwicklung*. **2009**, *Band 15*, 1–146. www.hessen-nanotech.de.

[7] G. Iyer, R. Gorur, R. Richert, A. Krivda, L. Schmidt, Dielectric Properties of Epoxy Based Nanocomposites for High Voltage Insulation, *IEEE Trans. Dielectr. Electr. Insul.* **2011**, *18*, 659–666. doi:10.1109/TDEI.2011.5931050.

[8] W. Evans, R. Prasher, J. Fish, P. Meakin, P. Phelan, P. Keblinski, Effect of aggregation and interfacial thermal resistance on thermal conductivity of nanocomposites and colloidal nanofluids, *Int. J. Heat Mass Transf.* **2008**, *51*, 1431–1438.

doi:10.1016/j.ijheatmasstransfer.2007.10.017.

[9] B.S. Rubin, Bisphenol A : An endocrine disruptor with widespread exposure and multiple effects, *J. Steroid Biochem. Mol. Biol.* **2011**, *127*, 27–34. doi:10.1016/j.jsbmb.2011.05.002.

[10] L.N. Vandenberg, R. Hauser, M. Marcus, N. Olea, W. V Welshons, Human exposure to bisphenol A (BPA), *Reprod. Toxicol.* **2007**, *24*, 139–177. doi:10.1016/j.reprotox.2007.07.010.

[11] European Commission, Proposed ban on the use of two-component epoxy containing bisphenol A or bisphenol Adiglcidyl ether in the moulding of new plastic pipes inside existing water suppl pipes, **2016**,. http://ec.europa.eu/growth/tools-databases/tris/en/search/?trisaction=search.detail&year=2015&num=677 (accessed January 18, 2017).

[12] V. Schenk, E. Rossegger, C. Ebner, F. Bangerl, K. Reichmann, B. Hoffmann, M. Höpfner, F. Wiesbrock, RGD-Functionalization of poly(2-oxazoline)-based networks for enhanced adhesion to cancer cells, *Polymers (Basel).* **2014**, *6*, 264–279. doi:10.3390/polym6020264.

[13] C. Petit, K.P. Luef, M. Edler, T. Griesser, J.M. Kremsner, A. Stadler, B. Grassl, S. Reynaud, F. Wiesbrock, Microwave-Assisted Syntheses in Recyclable Ionic Liquids: Photoresists Based on Renewable Resources, *ChemSusChem*. **2015**, *8*, 3401–3404. doi:10.1002/cssc.201500847.

[14] V. Schenk, L. Ellmaier, E. Rossegger, M. Edler, T. Griesser, G. Weidinger, F. Wiesbrock, Water-Developable Poly(2-oxazoline)-Based Negative Photoresists, *Macromol. Rapid Commun.* **2012**, *33*, 396–400. doi:10.1002/marc..201100717.

[15] H.C. Kolb, M.G. Finn, K.B. Sharpless, Click Chemistry: Diverse Chemical Function from a Few Good Reactions, *Angew. Chemie - Int. Ed.* **2001**, *40*, 2004–2021. doi:10.1002/1521-3773(20010601)40:11<2004::AID-ANIE2004>3.0.CO;2-5.

[16] R. Hoogenboom, Poly(2-oxazoline)s: A polymer class with numerous potential applications, *Angew. Chemie - Int. Ed.* **2009**, *48*, 7978–7994. doi:10.1002/anie.200901607.

[17] K. Dutta, S.K. De, Electrical conductivity and dielectric properties of SiO2 nanoparticles dispersed in conducting polymer matrix, *J. Nanoparticle Res.* **2007**, *9*, 631–638. doi:10.1007/s11051-006-9184-4.

[18] M.X. Shen, Y.X. Cui, J. He, Y.M. Zhang, Thermal conductivity model of filled polymer composites, *Int. J. Miner. Metall. Mater.* **2011**, *18*, 623–631. doi:10.1007/s12613-011-0487-9.

[19] Y.S. Perets, L.Y. Matzui, L.L. Vovchenko, Y.I. Prylutskyy, P. Scharff, U. Ritter, The effect of boron nitride on electrical conductivity of nanocarbon-polymer composites, *J. Mater. Sci.* **2014**, *49*, 2098–2105. doi:10.1007/s10853-013-7901-9.

[20] A. Fürst, Ernest Werner Siemens, Deutsche Verlags-Anstalt Stuttgard, **1916**,.

[21] N. Tesla, Electro Magnetic Motor, US-Patent 381,968, **1888**,.

[22] J.R. Lucas, E. Kuffel, W.S. Zaengl, High Voltage Engineering, Fundamentals, **2000**,. doi:10.1016/B978-075063634-6/50010-1.

[23] D.J. Holtzhausen, D.W. Vosloo, High Voltage Engineering Practice and Theory, **2003**, ISBN: 978-0-620-3767-7.

[24] J.M. Carrasco, L.G. Franquelo, J.T. Bialasiewicz, S. Member, E. Galván, R.C.P. Guisado, S. Member, M. Ángeles, M. Prats, J.I. León, N. Moreno-alfonso, Power-Electronic Systems for the Grid Integration of Renewable Energy Sources : A Survey, *Ieee Trans. Ind. Electron.* **2006**, *53*, 1002–1016. doi:10.1109/TIE.2006.878356.

[25] C.T. Dervos, C.D. Paraskevas, P.D. Skafidas, P. Vassiliou, A Complex Permittivity Based Sensor for the Electrical Characterization of High-Voltage Transformer Oils, *Sensors*. **2005**, *5*, 302–316. doi:10.3390/s5040302.

[26] R. Marenbach, D. Nelles, C. Tuttas, Elektrische Energietechnik, Springer Fachmedien Wiesbaden, **2013**,. doi:10.1007/978-3-8348-2190-4.

[27] R.B. Munn, Electric Power Generator and System, US-Patent 4.475.075, **1984**,.

[28] J.C. Botts, High voltage generator insulation, *IEEE Electr. Insul. Mag.* **1963**, 202–206.

[29] W.H.Y. Stress, Stress Grading for High Voltage, *IEEE Electr. Insul. Mag.* **1995**, *11*, 26–31.

[30] J. Alexander, T. Bertolini, Epoxide Reactions, *J. Chem. Educ.* **2002**, *79*, 1.

[31] W. Brostow, W. Chonkaew, K.P. Menard, T.W. Scharf, Modification of an epoxy resin with a fluoroepoxy oligomer for improved mechanical and tribological properties, *Mater. Sci. Eng. A*. **2009**, *507*, 241–251. doi:10.1016/j.msea.2008.12.008.

[32] T.W. Dakin, Application of Epoxy Resins in Electrical Apparatus, *IEEE Trans. Dielectr. Electr. Insul.* **1974**, *EI-9*, 121–128.

[33] R. Sarathi, R.K. Sahu, P. Rajeshkumar, Understanding the thermal, mechanical and electrical properties of epoxy nanocomposites, *Mater. Sci. Eng. A*. **2007**, *445–446*, 567–578. doi:10.1016/j.msea.2006.09.077.

[34] T. Tanaka, G.C. Montanari, R. Mulhaupt, Polymer nanocomposites as dielectrics and electrical insulation-perspectives for processing technologies, material characterization and future applications, *IEEE Trans. Dielectr. Electr. Insul.* **2004**, *11*, 763–784. doi:10.1109/TDEI.2004.1349782.

[35] B. Wetzel, P. Rosso, F. Haupert, K. Friedrich, Epoxy nanocomposites - fracture and toughening mechanisms, *Eng. Fract. Mech.* **2006**, *73*, 2375–2398. doi:10.1016/j.engfracmech.2006.05.018.

[36] M.R. Bockstaller, R.A. Mickiewicz, E.L. Thomas, Block copolymer nanocomposites: Perspectives for tailored functional materials, *Adv. Mater.* **2005**, *17*, 1331–1349. doi:10.1002/adma.200500167.

[37] T. Hanemann, D.V. Szabó, Polymer-Nanoparticle composites: From Synthesis to Modern Applications, *Materials (Basel).* **2010**, *3*, 3468–3517. doi:10.3390/ma3063468.

[38] S. Gabriel, Zur Kenntniss des Bromäthylamins, *Berichte Der Dtsch. Chem. Gesellschaft*. **1889**, *22*, 1139–1154.

[39] H.-J. Krause, P. Neumann, Verfahren zur Herstellung von 2-Alkyl- bzw. 2-Alkenyl- oxazolinen, EP 0 315 856 B1, **1995**,.

[40] H. Witte, W. Seeliger, Cyclische Imidsäureester aus Nitrilen und Aminoalkoholen, *Justus Liebigs Ann. Chem.* **1974**, *1974*, 996–1009. doi:10.1002/jlac.197419740615.

[41] A. Gress, A. Völkel, H. Schlaad, Thio-Click Modification of Poly [2- (3-butenyl) -2-oxazoline], *Macromolecules*. **2007**, *40*, 7928–7933. doi:10.1021/ma071357r.

[42] T.R. Dargaville, K. Lava, B. Verbraeken, R. Hoogenboom, Unexpected Switching of the Photogelation Chemistry When Cross-Linking Poly(2-oxazoline) Copolymers, *Macromolecules*. **2016**, *49*, 4774–4783. doi:10.1021/acs.macromol.6b00167.

[43] D.A. Tomalia, D.P. Sheetz, Homopolymerization of 2-alkyl- and 2-aryl-2-oxazolines, *J. Polym. Sci. Part A-1 Polym. Chem.* **1966**, *4*, 2253–2265. doi:10.1002/pol.1966.150040919.

[44] T. Kagiya, T. Maeda, K. Fukui, S. Narisawa, Ring Opening Polymerization Of 2-Substituted 2-Oxazolines\r, *Polym. Lett.* **1966**, *4*, 441–445. doi:10.1002/pol.1966.110040701.

[45] W. Seeliger, E. Aufderhaar, W. Diepers, R. Feinauer, R. Nehring, W. Thier, H. Hellmann, Recent Syntheses and Reactions of Cyclic Imidic Esters, *Angew. Chemie Int. Ed. English*. **1966**, *5*, 875–888.

doi:10.1002/anie.196608751.

[46] A. Levy, M. Litt, Polymerization Of Cyclic Imino Ethers. I. Oxazolines, *Polym. Lett.* **1967**, *5*, 871–879. doi:10.1002/pol.1967.110050927.

[47] N.E. Leadbeater, R. Hoogenboom, U.S. Schubert, F. Wiesbrock, Microwave-assisted Synthesis: General Concepts, in: Microwave-Assisted Polym. Synth., **2016**,: p. 357. doi:10.1007/12_2013_274.

[48] F. Wiesbrock, R. Hoogenboom, M. Leenen, S.F.G.M. Van Nispen, M. Van Der Loop, C.H. Abeln, A.M.J. Van Den Berg, U.S. Schubert, Microwave-Assisted Synthesis of a 4^2-Membered Library of Diblock Copoly (2-oxazoline)s and Chain-Extended Homo Poly (2-oxazoline)s and Their Thermal Characterization, *Macromolecules*. **2005**, *38*, 7957–7966. doi:10.1021/ma050437x.

[49] E. Rossegger, V. Schenk, F. Wiesbrock, Design strategies for functionalized poly(2-oxazoline)s and derived materials, *Polymers (Basel).* **2013**, *5*, 956–1011. doi:10.3390/polym5030956.

[50] C. Ebner, T. Bodner, F. Stelzer, F. Wiesbrock, One decade of microwave-assisted polymerizations: Quo vadis?, *Macromol. Rapid Commun.* **2011**, *32*, 254–288. doi:10.1002/marc.201000539.

[51] F. Wiesbrock, R. Hoogenboom, C.H. Abeln, U.S. Schubert, Single-mode microwave ovens as new reaction devices: Accelerating the living polymerization of 2-ethyl-2-oxazoline, *Macromol. Rapid Commun.* **2004**, *25*, 1895–1899. doi:10.1002/marc.200400369.

[52] R. Hoogenboom, M.W.M. Fijten, H.M.L. Thijs, B.M. Van Lankvelt, U.S. Schubert, Microwave-assisted synthesis and properties of a series of poly (2-alkyl-2-oxazoline) s, *Desgined Monomers Polym.* **2005**, *8*, 659–671. doi:10.1163/156855505774597704.

[53] M. Glassner, D.R. D'Hooge, J. Young Park, P.H.M. Van Steenberge, B.D. Monnery, M.F. Reyniers, R. Hoogenboom, Systematic investigation of alkyl sulfonate initiators for the cationic ring-opening

polymerization of 2-oxazolines revealing optimal combinations of monomers and initiators, *Eur. Polym. J.* **2015**, *65*, 298–304. doi:10.1016/j.eurpolymj.2015.01.019.

[54] M. Fimberger, K. Luef, C. Payerl, R. Fischer, F. Stelzer, M. Kállay, F. Wiesbrock, The Π-Electron Delocalization in 2-Oxazolines Revisited: Quantification and Comparison with Its Analogue in Esters, *Materials (Basel).* **2015**, *8*, 5385–5397. doi:10.3390/ma8085249.

[55] J.M. Kranenburg, C.A. Tweedie, R. Hoogenboom, F. Wiesbrock, H.M.L. Thijs, C.E. Hendriks, K.J. Van Vliet, U.S. Schubert, Elastic moduli for a diblock copoly(2-oxazoline) library obtained by high-throughput screening, *J. Mater. Chem.* **2007**, *17*, 2713–2721. doi:10.1039/b701945a.

[56] R. Hoogenboom, F. Wiesbrock, H. Huang, M.A.M. Leenen, H.M.L. Thijs, S.F.G.M. Van Nispen, M. Van Der Loop, C.A. Fustin, A.M. Jonas, J.F. Gohy, U.S. Schubert, Microwave-assisted cationic ring-opening polymerization of 2-oxazolines: A powerful method for the synthesis of amphiphilic triblock copolymers, *Macromolecules*. **2006**, *39*, 4719–4725. doi:10.1021/ma060952a.

[57] M.W.M. Fijten, J.M. Kranenburg, H.M.L. Thijs, R.M. Paulus, B.M. Van Lankvelt, J. De Hullu, M. Springintveld, D.J.G. Thielen, C.A. Tweedie, R. Hoogenboom, K.J. Van Vliet, U.S. Schubert, Synthesis and Structure - Property Relationships of Random and Block Copolymers: A Direct Comparison for Copoly (2-oxazoline)s, *Macromolecules*. **2007**, *40*, 5879–5886.

[58] J.M. Stubbs, D.C. Sundberg, Morphologies of spin-coated films of a library of diblock copoly(2-oxazoline)s and their correlation to the corresponding surface energies, *J. Polym. Sci. Part B Polym. Phys.* **2006**, *43*, 2790–2806. doi:10.1002/10.1002/polb.20558.

[59] K. Kempe, E.F.-J. Rettler, R.M. Paulus, A. Kuse, R. Hoogenboom, U.S. Schubert, A systematic investigation of the effect of side chain branching on the glass transition temperature and mechanical

properties of aliphatic (co-)poly(2-oxazoline)s, *Polymer (Guildf).* **2013**, *54*, 2036–2042. doi:10.1016/j.polymer.2013.01.016.

[60] K. Kempe, S. Jacobs, H.M.L. Lambermont-Thijs, M.M.W.M. Fijten, R. Hoogenboom, U.S. Schubert, Rational design of an amorphous poly(2-oxazoline) with a low glass-transition temperature: Monomer synthesis, copolymerization, and properties, *Macromolecules*. **2010**, *43*, 4098–4104. doi:10.1021/ma9028536.

[61] C.E. Hoyle, C.N. Bowman, Thiol-En-Klickchemie, *Angew. Chemie*. **2010**, *122*, 1584–1617. doi:10.1002/ange.200903924.

[62] M. Fimberger, V. Schenk, E. Rossegger, F. Wiesbrock, UV-Induced Crosslinking of Poly[2-(2'-Norbornenyl)-2-Oxazoline]s, *Period. Polytech. Chem. Eng.* **2014**, *58*, 69. doi:10.3311/PPch.7206.

[63] K. Kempe, A. Vollrath, H.W. Schaefer, T.G. Poehlmann, C. Biskup, R. Hoogenboom, S. Hornig, U.S. Schubert, Multifunctional poly(2-oxazoline) nanoparticles for biological applications, *Macromol. Rapid Commun.* **2010**, *31*, 1869–1873. doi:10.1002/marc.201000283.

[64] J. Rueda, R. Suica, H. Komber, B. Voit, Synthesis of new polymethyloxazoline hydrogels by the "macroinitiator" method, *Macromol. Chem. Phys.* **2003**, *204*, 954–960. doi:10.1002/macp.200390065.

[65] K.P. Luef, C. Petit, B. Ottersböck, G. Oreski, F. Ehrenfeld, B. Grassl, S. Reynaud, F. Wiesbrock, UV-mediated thiol-ene click reactions for the synthesis of drug-loadable and degradable gels based on copoly(2-oxazoline)s, *Eur. Polym. J.* **2017**, *88*, 701–712. doi:10.1016/j.eurpolymj.2016.08.012.

[66] T.R. Dargaville, R. Forster, B.L. Farrugia, K. Kempe, L. Voorhaar, U.S. Schubert, R. Hoogenboom, Poly(2-oxazoline) hydrogel monoliths via thiol-ene coupling, *Macromol. Rapid Commun.* **2012**, *33*, 1695–1700. doi:10.1002/marc.201200249.

[67] A.M. Kelly, A. Hecke, B. Wirnsberger, F. Wiesbrock, Synthesis of Poly (2-oxazoline) -Based Hydrogels with Tailor-Made Swelling Degrees Capable of Stimuli-Triggered Compound Release, *Macromol. Rapid Commun*. **2011**, *32*, 1815–1819.

[68] T.R. Dargaville, B.G. Hollier, A. Shokoohmand, R. Hoogenboom, Poly(2-oxazoline) hydrogels as next generation three-dimensional cell supports, *Cell Adhes. Migr.* **2014**, *8*, 88–93. doi:10.4161/cam.28205.

[69] M. Fimberger, I.A. Tsekmes, R. Kochetov, J.J. Smit, F. Wiesbrock, Crosslinked poly(2-oxazoline)s as “green” materials for electronic applications, *Polymers (Basel).* **2016**, *8*, 1–12. doi:10.3390/polym8010006.

[70] M.H. Litt, C.S. Lin, Selective hydrolysis of oxazoline block copolymers, *J. Polym. Sci. Part A Polym. Chem.* **1992**, *30*, 779–786. doi:10.1002/pola.1992.080300507.

[71] S. Navarro, A. Shkilnyy, B. Tiersch, A. Taubert, H. Menzel, Preparation, Characterization, and Thermal Gelation of Amphiphilic Alkyl-poly(ethyleneimine), *Langmuir*. **2009**, *25*, 10558–10566. doi:10.1021/la9013569.

[72] H.P.C. Van Kuringen, J. Lenoir, E. Adriaens, J. Bender, B.G. De Geest, R. Hoogenboom, Partial Hydrolysis of Poly(2-ethyl-2-oxazoline) and Potential Implications for Biomedical Applications?, *Macromol. Biosci.* **2012**, *12*, 1114–1123. doi:10.1002/mabi.201200080.

[73] J.M. Havard, M. Yoshida, D. Pasini, N. Vladimirov, J.M.J. Fréchet, S. Yamada, K. Patterson, D.R. Medeiros, C.G. Willson, J.D. Byers, Design of Photoresists with Reduced Environmental Impact. 1. Water-Soluble Resists Based on Photo-Cross-Linking of Poly(2-Isopropenyl-2-oxazoline), *J. Polym. Sci. Part A Polym. Chem.* **1999**, *37*, 1225–1236. doi:10.1021/cm980603y.

[74] M. Fimberger, A. Behrendt, G. Jakopic, F. Stelzer, V. Kumbaraci, F. Wiesbrock, Modification Pathways for Copoly(2-oxazoline)s Enabling

Their Application as Antireflective Coatings in Photolithography, *Macromol. Rapid Commun.* **2016**, *37*, 233–238. doi:10.1002/marc.201500589.

[75] G. Klancnik, J. Medved, P. Mrvar, Differential thermal analysis (DTA) and differential scanning calorimetry (DSC) as a method of material investigation, *Mater. Geoenvironmentent*. **2010**, *57*, 127–142.

[76] P. Preetha, M.J. Thomas, AC breakdown characteristics of epoxy nanocomposites, *IEEE Trans. Dielectr. Electr. Insul.* **2011**, *18*, 1526–1534. doi:10.1109/TDEI.2011.6032821.

[77] T. Andritsch, R. Kochetov, Y.T. Gebrekiros, U. Lafont, P.H.F. Morshuis, J.J. Smit, Synthesis and dielectric properties of epoxy based nanocomposites, *2009 IEEE Conf. Electr. Insul. Dielectr. Phenom.* **2009**, 523–526. doi:10.1109/CEIDP.2009.5377771.

[78] E. Kuffel, W.S. Zaengl, J. Kuffel, Non-destructive insulation test techniques, in: High Volt. Eng. Fundam., **2000**,: pp. 395–459. doi:10.1016/B978-075063634-6/50008-3.

[79] F. Hussain, J. Chen, M. Hojjati, Epoxy-silicate nanocomposites: Cure monitoring and characterization, *Mater. Sci. Eng. A*. **2007**, *445–446*, 467–476. doi:10.1016/j.msea.2006.09.071.

[80] E.I. Izgorodina, M. Forsyth, D.R. Macfarlane, On the components of the dielectric constants of ionic liquids: ionic polarization?, *Phys. Chem. Chem. Phys.* **2009**, *11*, 2452–2458. doi:10.1039/b815835e.

[81] S. Wijnans, B.J. De Gans, F. Wiesbrock, R. Hoogenboom, U.S. Schubert, Characterization of a poly(2-oxazoline) library by high-throughput, automated contact-angle measurements and surface-energy calculations, *Macromol. Rapid Commun.* **2004**, *25*, 1958–1962. doi:10.1002/marc.200400408.

[82] F. Hejda, P. Solar, J. Kousal, Surface Free Energy Determination by Contact Angle Measurements – A Comparison of Various Approaches,

WDS'10 Proc. Contrib. Pap. **2010**, 25–30.

[83] A. Mattiuzzi, I. Jabin, C. Mangeney, C. Roux, O. Reinaud, L. Santos, J.-F. Bergamini, P. Hapiot, C. Lagrost, Electrografting of calix[4]arenediazonium salts to form versatile robust platforms for spatially controlled surface functionalization, *Nat. Commun.* **2012**, *3*, 1130. doi:10.1038/ncomms2121.

[84] D.K. Owens, R.C. Wendt, Estimation of the surface free energy of polymers, *J. Appl. Polym. Sci.* **1969**, *13*, 1741–1747. doi:10.1002/app.1969.070130815.

[85] J. Ford, Thermal Analysis — Fundamentals and Applications to Polymer Science, 2nd Edition, Edited by T. Hatakeyama and F.X. Quinn, Wiley, Chichester, 1999, viii+180 pages. ISBN 0-471-98362-4; £55.00, **2000**,. doi:10.1016/S0039-9140(99)00304-5.

[86] J.F. Fu, L.Y. Shi, Q.D. Zhong, Y. Chen, L.Y. Chen, Thermally conductive and electrically insulative nanocomposites based on hyperbranched epoxy and nano-Al 2O 3 particles modified epoxy resin, *Polym. Adv. Technol.* **2011**, *22*, 1032–1041. doi:10.1002/pat.1638.

[87] X. Ma, K.M.B. Jansen, L.J. Ernst, W.D. van Driel, O. van der Sluis, G.Q. Zhang, Characterization of moisture properties of polymers for IC packaging, *Microelectron. Reliab.* **2007**, *47*, 1685–1689. doi:10.1016/j.microrel.2007.07.090.